D I P L O M A R B E I T

Sustainable Functionalization of Lignin for the Production of Biocolloids

Ausgeführt am Institut für Chemie nachwachsender Rohstoffe
der Universität für Bodenkultur Tulln

Unter der Anleitung von Univ.Prof. Dipl.-Chem. Dr.rer.nat. DDr.h.c. Thomas Rosenau und Dr. Marco Beaumont als verantwortlich mitwirkenden Universitätsassistenten (BOKU Tulln) sowie Ao.Univ.Prof Dipl.-Ing. Dr.techn. Ewald Srebotnik (TU Wien)

durch

Maximilian Lubitz

_____   _____
Datum   Unterschrift (Student)

Kurzfassung

Fossile gegen erneuerbare Rohstoffe zu ersetzen war schon immer eine herausfordernde Aufgabenstellung in der Menschheitsgeschichte. Lignocellulose, bestehend aus Cellulose, Hemicellulose und Lignin stellt das strukturelle Grundgerüst von vaskulären Pflanzen dar und besitzt zudem Kohlenstoff in großer Menge. Deswegen ist Lignocellulose ideal für den Einsatz als erneuerbare Ressource geeignet. Besonders das Biopolymer Lignin ist sehr reich an aromatischen Einheiten, wodurch die Umsetzung zu höherwertigen Produkten erleichtert wird.

Für diesen Zweck sind Acetylierung und Esterifizierung häufig genutzte Methoden. Zum heutigen Stand der Technik werden jedoch die dafür genutzten Prozesse unter harschen Bedingungen wie hohe Temperaturen und Drücke sowie mit gefährlichen Chemikalien durchgeführt. Um diese Nachteile für die Acetylierung zu überwinden, wurden Feststoff-Feststoff Reaktionen in einer Kugelmühle durchgeführt und die dazugehörigen Parameter (Feuchtigkeitsgehalt, Reaktionszeit und Menge an *N*-Acetylimidazol), bezogen auf den Substitutionsgrad, optimiert. Für die Esterifizierung wurden *in situ* Synthesen mit unterschiedlichen Anhydriden und Imidazol durchgeführt, sodass *N*-Acylimidazole und anschließend Ligninester mit verschiedenen Größen und Längen erhalten werden konnten.

Des Weiteren wurden Nanopartikel von einer Reihe ausgewählter Ligninester hergestellt und der Einfluss der funktionellen Gruppen sowie des Substitutionsgrades auf die Benetzbarkeit, Oberflächenspannung, Morphologie, kolloidale Stabilität und Größe untersucht.

Abstract

Replacing the fossil by a renewable feedstock has been a highly challenging task in human history. Lignocellulose, consisting of cellulose, hemicellulose and lignin, provides the structural framework of vascular plants and offers an abundant source of carbon. Therefore, lignocellulose is suitable for its application as renewable resource. In particular, the biopolymer lignin is very rich in aromatic units, which facilitates synthesis into tailored and value-added products.

For this purpose acetylation and esterification are commonly used methods, but state of the art processes apply harsh conditions. Besides high pressures and temperatures, hazardous chemicals are used as well. To overcome these drawbacks for the acetylation, solid-solid reactions of lignin and *N*-acetylimidazole were performed in a ball mill and the corresponding parameters (moisture content, reaction time, amount of *N*-acetylimidazole) were optimized referred to the degree of substitution. For the esterification, solvent-free *in situ* syntheses with varying anhydrides and imidazole were carried out in order to obtain *N*-acylimidazoles and subsequently lignin esters with varying size and length.

Moreover, nanoparticles were prepared for a selected number of lignin esters and the influence of the functional group as well as the degree of substitution on wettability, surface tension, morphology, colloidal stability and size was studied.

Acknowledgements

I would like to express my special thanks to my supervisor Prof. Thomas Rosenau for the chance to perform the diploma thesis in his research group at BOKU Tulln as well as his support.

I am also very thankful to Dr. Marco Beaumont and Dr. Irina Sulaeva for their excellent guidance, encouragement and help throughout the last months.

Special thanks to Prof. Ewald Srebotnik from the TU Vienna for the support and organization and making this thesis possible as cooperation in between two universities.

Furthermore, I want to thank all members of the renewable resources department for an incredible working atmosphere and being supportive at all times. I appreciated conversations and experiences at lunch breaks or table soccer tournaments a lot.

I am very grateful to my family for their mental and financial support during my last years of study. Last but not least, I would like to thank my friends for making my time at university unforgettable.

List of abbreviations

AA	acetic anhydride
AcOH	acetic acid
AFM	atomic force microscopy
ATR	attenuated total reflection
CO_2	carbon dioxide
DI	deionized
DLS	dynamic light scattering
DMSO	dimethyl sulfoxide
DoE	Design of Experiment
DS	degree of substitution
Eq	equivalents
FTIR	Fourier transformed infrared spectroscopy
G	guaiacyl unit
H	high degree of substitution
H	p-hydroxyphenyl unit
HA	hexanoic anhydride
HH	very high degree of substitution
IBA	isobutyric anhydride
Im	imidazole
$LiTaO_3$	lithium tantalate
LNP	lignin nanoparticle
M	medium degree of substitution
NMR	nuclear magnetic resonance spectroscopy
NP	nanoparticle
R1	response (degree of substitution)
RI	refractive index
RT	room temperature
S	syringyl unit
SD	standard derivation
SiO_2	silicium dioxide
θ	contact angle
UV-VIS	ultraviolet – visible spectroscopy
ZnSe	zinc selenide

Contents

1 Introduction

Still, fossil feedstocks are substantial sources in modern society. Besides energy supply they are essential for the manufacture of important products like chemicals, fuels and materials. Nevertheless, the growing global population and the rise in CO_2 anthropogenic emissions necessitate alternatives for these finite resources (Dapsens et al., 2012; Sabine et al., 2004).

1.1 Biorefinery concept

Biorefineries target to maximize outputs by processing raw materials comparable to conventional refineries but with pivotal difference of using biomass (Lin et al., 2013). Biomass is characterized as "biological material derived from living or recently living organisms" (Khan et al., 2009). Clark et al. (H. Clark et al., 2009) describe biomass as "the only sustainable alternative to fossil fuels as a source of carbon for our chemical and material needs", which does not compete with food production. Besides its abundant source of carbon it is inexpensive, renewable and CO_2-neutral. On the other hand, products of naturally grown resources show several drawbacks in contrast to products of synthetic resources, such as higher humidity absorption, poor fire resistance, reduced durability and mechanical properties, price and qualitative fluctuation, and obstacles applying established manufacturing methods (Dittenber and GangaRao, 2012). Therefore it is a very challenging task to replace the fossil by a renewable feedstock.

1.2 Native lignin

However, among various types of biomass (Huber and Corma, 2007), lignocellulose is considered as the most promising raw material for prospective biorefinery (Anwar et al., 2014; Dapsens et al., 2012). It is the major structural component of wood and straw and forms the structural support system in all vascular plants. Lignocellulose consists of cellulose, hemicellulose (carbohydrates) and lignin, which are widely distributed throughout the vegetation. The composition of lignocellulose varies for different species. For wood it is determined as 45-55% cellulose, 25-40% hemicellulose and 20-35% lignin. Notably, the lignin content in softwoods is higher compared to hardwoods, whereas hardwood contains more cellulose and hemicellulose (Betts et al., 1991). Lignocellulose could be comprehensive regenerated on global scale. Currently, most biorefineries focus on the carbohydrate

fractions while not fully exploiting the potential of the second most abundant terrestrial polymer, lignin (H. Wang et al., 2019). For example, the first generation bioethanol production generates about 60% more lignin than necessary, which is solely used to cover the internal energy supply by combustion (Ragauskas et al., 2014). Furthermore, lignin represents the primary renewable resource attributed to aromatic units (Lievonen et al., 2016). Thus, lignin enhancement via transformation into value-added products is of pivotal significance (H. Wang et al., 2019).

Native lignin is vital for *plantae* as it adds strength to the cell wall, controls the fluid flow, protects against biochemical attacks and assists the exposure to different climates (Vance et al., 1980; Wang et al., 2018). Hence lignin provides essential structural properties for plants. (Boerjan et al., 2003). It "is mostly present in the middle lamella between wood cells and the secondary cell wall" (Lievonen et al., 2016) and the chemical structure of native lignin depends on ecological factors such as plant growth, climate, nutrition and illumination (Hatfield and Vermerris, 2001). Moreover, lignin can be distinguished depending on its type by means of functional groups and molecular weight (Upton and Kasko, 2016). Because of this variety, it is very difficult to analyze and interpret its structure completely, although the main chemical constituents remain the same. In general, lignin is an amorphous, highly branched, and three dimensional network biomacromolecule, the monomer units of which are linked via diverse bonds including carbon–carbon and ether linkages (Ahvazi et al., 2016; Gao and Fatehi, 2019; Tang et al., 2020).
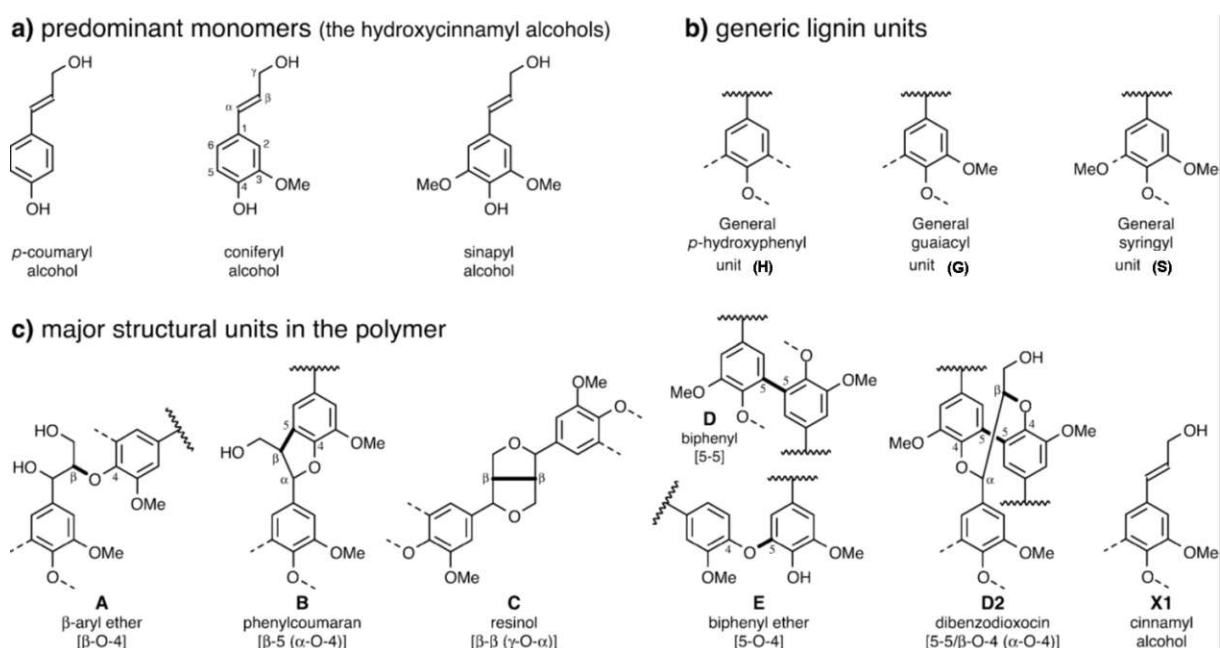
Figure 1: (a) *p*-Hydroxycinnamyl alcohols as predominant lignin monomers, the lignin precursors or monolignols. **(b)** Corresponding polymer generic or basic units. **(c)** Major

structural units in the lignin polymer. The numbering follows that in a review (Boerjan et al., 2003). The bolded bonds are formed in the radical coupling reaction. This figure was modified from (Ralph et al., 2004).

The predominant monomers for lignification are the three *p*-hydroxycinnamyl alcohols: *p*-coumaryl alcohol, coniferyl alcohol, and sinapyl alcohol. They show varying degree of methoxylation and function as precursors for lignin in regards to radical polymerization (see Figure 1a). In the lignin polymer the corresponding basic units (generic units Figure 1b) of the monomeric lignin precursors, or monolignols, vary widely depending on the plant species. Thus, softwood is mainly constituted of guaiacyl units (G), hardwood of G and syringyl (S) units, while herbaceous plant of G-S and p-hydroxyphenyl (H) units (Huang et al., 2019). The driving force of radical biosynthesis of lignin is to form monolignol radicals with several resonance structures, which react in a free radical polymerization resulting in a range of structural units in the polymer (Figure 1c) (Bertella and Luterbacher, 2020; Ralph et al., 2004; Rodrigues Mota et al., 2018). Therefore, lignin has been referred to as supramolecular self-assembled chaos (Achyuthan et al., 2010). Nevertheless, Ralph et al. (Ralph et al., 2019) worked out representative 20-mer models of native lignin's bewildering and complex structures for the three major plant classes (gymnosperm/softwood, angiosperm/dicot/hardwood and monocot), which is shown in Figure 2.
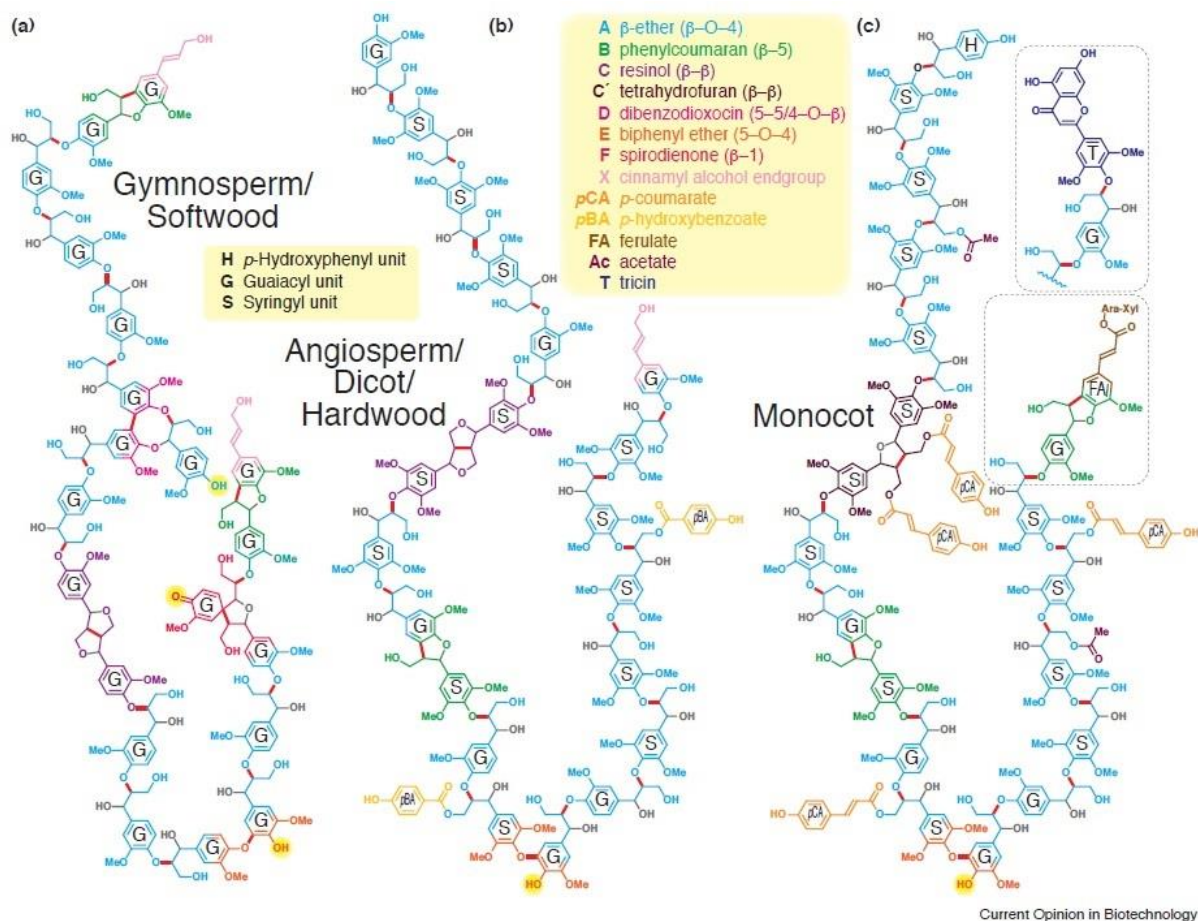
Figure 2: Lignin 20-mer model structures. for: (a) A gymnosperm/softwood, (b) An angiosperm/dicot/hardwood, and (c) A monocot. The generic units and chemical components (colored) of the different lignins are listed with their corresponding abbreviations respectively (Ralph et al., 2019)

The authors note that the native lignin model structure details in Figure 2 "have been drawn based on the best current information and with rigorously followed concepts". However, limitations in analytical fittings perforce occurred, such as the spirodienone unit **F** (just 1-2%), yet it was depicted in the softwood structure (a). Among other linkages, radical lignification result in either β-O-4 (most abundant) bonds, or in other inter unit linkages such as β-5, β-β, 5-5, 4-O-β and β-1 connections, due to the conjugated π-system. Consequently, diverse chemical components develop during polymerization (cf. marked structures in Figure 2) (Ralph et al., 2019). Great structural differences occur after biomass processing – during lignin extraction and recovery. Hence, technically processed lignins demonstrate a reduction in aliphatic hydroxyl groups, oxygenated aliphatic segments (β-O-4 units particularly), as well as a rise in aromatic hydroxyl groups, COOR and saturated aliphatic segments. Moreover, technical lignins undergo degradation, demethylation, and condensation

(Balakshin and Capanema, 2015). Kraft lignin is an example for technically processed lignin and therefore illustrated in Figure 3
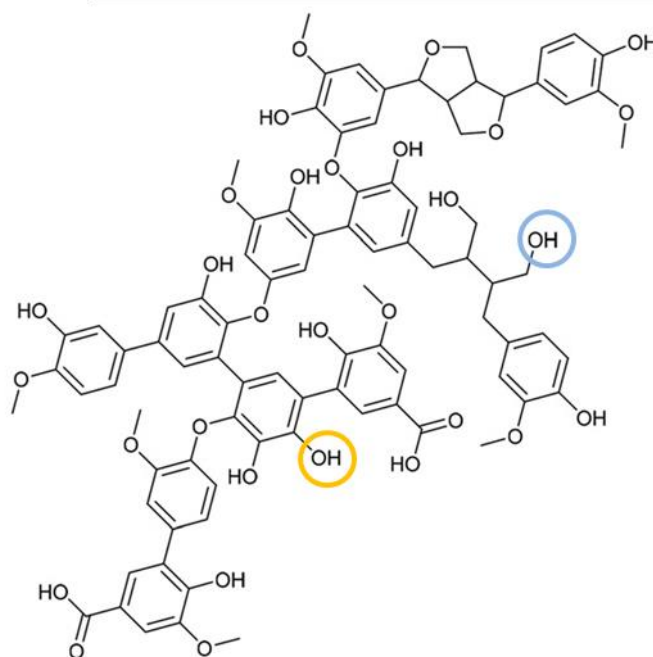
Figure 3: Fraction of acetone soluble kraft lignin with highlighted aliphatic (blue) and aromatic (orange) hydroxyl groups (Crestini et al., 2017)

The acetone soluble kraft lignin fraction in Figure 3 shows the differences of technical lignin compared to native lignin described above (cf. Figure 2 and Figure 3) as well as highlighted aromatic and aliphatic hydroxyl groups (most reactive functional groups) (Antonino et al., 2021). Thielemans and Wool (Thielemans and Wool, 2005) studied the nucleophilic reactivity of these alcohols for catalytic butyration and methacrylation lignin reactions with anhydrides and determined that the aromatic (phenolic) hydroxyl groups react three times faster than the aliphatic ones. Thus, higher functional group acidity results in faster nucleophilic reactions for lignin hydroxyl groups.

1.3 Biomass processing strategies

Before valorization or modification of biomass components, the biomacromolecules must be isolated (Hassan et al., 2018). During isolation and purification of cellulose, lignin arises on large scale as an unexploited byproduct for the pulp and paper industry (Carvajal et al., 2016). Owing to its high calorific value, industrial lignin is mostly used for burning. Just 5% is utilized for value-added products (Lievonen et al., 2016). In general, industrial or technical lignin can be classified into 4 major categories: Kraft, lignosulfonate (also known as sulfonated lignin), organosolv, and

soda lignin, with the latter two being produced by sulfur-free processes (Doherty et al., 2011).

About 50-70 million tons of lignin is manufactured per year (Saratale et al., 2019) whereby the supply capacity of lignosulfonates dominates the market, currently. However, Kraft lignin exhibit lower costs and greater reactivity. Hence the Kraft lignin market is growing faster between 2023 and 2028 and will compete reasonably (Dessbesell et al., 2020). These two lignin categories are obtained by the two key industrial processes: the sulfite and the Kraft process. Both fractionation techniques are based on the precipitation of the carbohydrate fraction, while dissolute and remove lignin. The Kraft lignin process is carried out at strong basic conditions using appropriate alkalis in order to break the ester bonds of hemicellulose and lignin polymers. Overall, drastic conditions are applied causing irreversible reactions which change the structure of the isolated lignin. Kraft lignin is therefore extremely modified, hydrophobic and has lower molecular weight compared to native lignin (Li et al., 2015).

The sulfite pulping process, conducted in acidic conditions, includes cracking of ether bonds and origination of carbon-carbon bonds. During ether cleavage carbocations are formed which further convert to lignosulfonates in the presence of bisulfite ions (R-O-R' + H^+ $\rightarrow$ R^+ + R'OH; R^+ + HSO_3^- $\rightarrow$ R-SO_3H). Subsequently, calcium hydroxide is added to the pulp to obtain sulfonated lignin (Li et al., 2015). Lignosulfonates possess higher average molecular weight compared to kraft lignin and good aqueous solubility (Figueiredo et al., 2018). However, these two major lignin feedstocks (on industrial scale) are not the optimal source in prospective biorefinery on ground of complex processes, high structural changes and large volume of generated wastewater (Li et al., 2015). Another isolation method which extracts lignin from biomass feedstock is the organosolv fractionation. It is carried out under mild conditions and the utilization of organic solvents such as primary alcohols (Li et al., 2015). Basically, the organosolv treatment cleaves the ether bonds and forms new phenolic groups. The resulting lignin obtains a lower molecular weight and a relatively high purity (Haq et al., 2020). The main drawback is the difficulty to perform the process on a large scale because of the enormous corrosion of device (Liao et al., 2020).

Besides processes isolating technical lignin a large number of alternative extraction methods exist (Margarida Martins et al., 2022) such as the Björkman process, which

enables a mild extraction of lignin from ball milled wood using neutral solvents (Guerra et al., 2006). Hence little structural change of the so called milled wood lignin (MWL) occurs. The structure of MWL is even regarded as the most identical to the native lignin. On the other hand, extensive ball milling causes side-chain oxidation and possible depolymerization as well as poor extraction yield (25-50% of theoretically available amount) (Hu et al., 2006). Therefore new free-phenolic hydroxyl groups are formed and the milled wood lignin does not represent the whole lignin, respectively (Li et al., 2015; Ragauskas et al., 2014).

In short, different isolation methods lead to different properties of lignin thus the type of lignin has to be taken into consideration for subsequent valorization.

1.4 Lignin valorization

Of course, the economic factor also has to be taken into account, especially for industrial usability. The costs and the availability of the isolated lignin in the market are consequently the decisive factors for the production of value-added products (Behling et al., 2016). Concerning this matter, the real and potential lignin market value for its value-added utilization in different chemicals/materials is correlated to the lignin production every year and is described in Figure 4 (Gosselink, 2011).
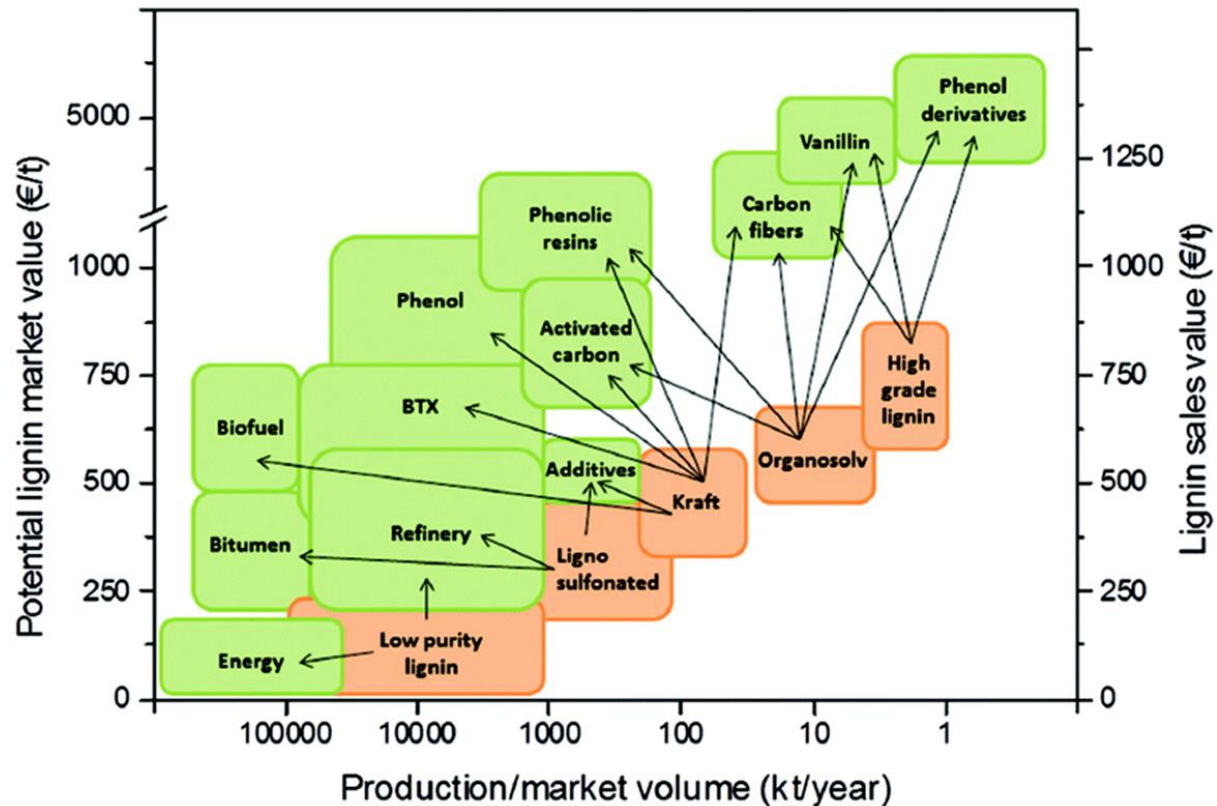

Figure 4: Actual lignin sales value for extracted lignin (orange) and corresponding potential lignin market value for value-added chemicals/materials (green)). Product combinations are

indicated by arrows. BTX is the abbreviation for benzene, toluene and xylene (Behling et al., 2016).

The enormous ecological potential for value-added lignin chemicals and materials is shown in Figure 4 . The arrows from extracted lignins (orange) to value-added products (green) indicate the potential of market value. For near horizontal arrows the value increment is limited but for ascending oblique or vertical arrows a substantial value increment is anticipated (Gosselink, 2011). Therefore, it has to be considered that the demand for a specific extracted lignin can increase rapidly in case of an improvement of a value-added lignin product (Behling et al., 2016).

1.5 Esterification of lignin

Esterification and especially acetylation are convenient and widely used modification methods in order to achieve value-added products of lignin (Glasser and Jain, 1993). Lignin acetates possess superior solubility characteristics and thus are used for structural analytics routinely (C. Wang et al., 2016). A systematical study of the influence of kraft lignin esters chain length from lignin acetate (C_2) to lignin stearate (C_{18}) on their solubility and thermal properties revealed their possible industrial use as plasticizers and internal mold lubricants (Lewis et al., 1943). Tinnemans and Greidanus (Tinnemans and Greidanus, 1984) used acetylated kraft lignin as compatibilizers (blends of low-density polyethylene and polypropylene) for recycled fractions of household waste achieving good tensile strength. Thielemans and Wool (Thielemans and Wool, 2005) analyzed the impact of acetylated kraft lignin as well as propionic, butyric and methacrylated kraft lignin esters on their solubility and reaction progression using theoretical predictions. It was concluded that n-butyric and hybrids of n-butyric/methacrylate can be incorporated in unsatured thermosetting composites due to their solubility in styrene.

On the other hand, the esterification methods described above are carried out under high pressures and temperatures consuming hazardous solvents either during preparation or purification. Mixtures of acyl chloride with pyridine or triethylamin were used for synthesis, and for example petroleum ether or benzene for purification at temperatures up to 90°C for the pioneering solubility exploration of Lewis et al. (Lewis et al., 1943). Glasser and Jain (Glasser and Jain, 1993) performed esterification either with equimolar pyridine/acyl chloride or acyl anhydride/acyl acid and sodium alkanoate as catalyst at temperatures up to approximately 200°C. The implementation of *N*-methylimidazole as catalyst improved the synthesis drastically

as it offered a complete reaction in approximately 1 h whereas reactions with pyridine took up to 48 h (Thielemans and Wool, 2004). Thielemans and Wool (Thielemans and Wool, 2005) used *N*-methylimidazole as catalyst combined with an equimolar mixture of acyl anhydride/acyl acid for synthesis with 1,4-dioxane as solvent and an applied temperature of 50 °C.

To sum up, lignin represents a low cost waste, non-toxic, low price bioresource and is an abundant source of saturated and unsaturated carbon units. It should not be surprising that it can be used in many applications, e.g., in biofuels (diesel, gas), additive (dispersant, filler), "agriculture (controlled release of pesticides and herbicides, sequestering agents for heavy metal, as component for humic acids formation in soil structures and as high-value fertilizers)", medical application ("drug encapsulation and delivery, treatment of obesity, diabetes, thrombosis, viruses and cancer"), as well as in cosmetics as UV-protectant and batteries (Behin and Sadeghi, 2016; Figueiredo et al., 2018; Gilca et al., 2015; Kai et al., 2016; Schneider et al., 2021, 2019; Vinardell and Mitjans, 2017).

1.6 Lignin nanoparticles as a value-added product

"Large particle size, heterogeneity, poor dispersibility and irregular morphology" are the limiting factors for the use of lignin as value-added materials (Schneider et al., 2021; B. Wang et al., 2019). Lignin based nanomaterials, for example, is one possibility to overcome some of these hindrances (Figueiredo et al., 2018). For viable biorefineries the conversion from lignin to value-added materials on nanoscale has been viewed as crucial (Liu et al., 2019a; Schneider et al., 2021). Lignin nanoparticles (LNPs, lignin NPs) are "green", easy biocompatible and inexpensive functional nanomaterials which can be applied in "thermoplastics, nanocomposites, foams, bactericides, products that require protection from UV radiation", etc. (Österberg et al., 2020; Schneider et al., 2021; X. Wang et al., 2016). It is assumed that nanoparticles are degradable (by microorganisms) or at least compostable (Österberg et al., 2020), but this may vary significantly depending on the lignin type and chemistry used. Yet, most biodegradability tests are solely run under aerobic conditions, hence these studies are difficult to assess (Iwata, 2015). In general, the synthesis of lignin nanoparticles should be complying with the principles of green chemistry (Schneider et al., 2021).

Biomolecule nanoparticles such as LNPs "provide new materials that combine the unique optical, electronic, catalytic etc. properties of the nanoelements with the

recognition or biocatalytic functions of biomolecules" (Willner and Willner, 2010). Further, they simply offer advantages compared to bulk materials, due to the expanded surface to volume ratio. The preparation of new desirable properties occurring only when raw material is arranged on nanoscale (Zhang et al., 2021) therefore supply a wide range of applications for lignin NPs, such as antioxidant (Trevisan and Rezende, 2020), dispersant, coating and paint (Österberg et al., 2020), tissue engineering (Kai et al., 2016), encapsulating of hydrophobic molecules (Dai et al., 2017), dye removal (Azimvand et al., 2018), food packaging (Yang et al., 2016), wound dressing (Reesi et al., 2018) many others (Schneider et al., 2021).

1.7 Lignin nanoparticles fabrication

LNPs can be synthesized by controllable and simple processes which usually provide uniform (despite native heterogeneity and complexity of lignin) nanoparticles with regular structures when lignin solution is added to an antisolvent continuously. (Tian et al., 2017). The schematic formation of LNPs is given in Figure 5
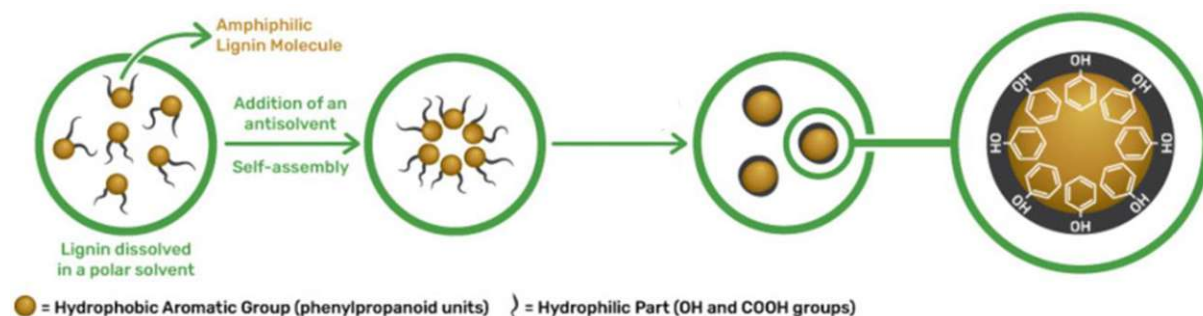
Figure 5: Schematic figure explaining the formation of lignin nanoparticles (Schneider et al., 2021).

Lignin possesses amphiphilic properties, comprised by the hydrophobic part (phenylpropanoid units) and hydrophilic part (hydroxyl and carboxyl groups) thus nanoparticles can be formed (see Figure 5). It is considered that, comparable to micelles, the hydrophobic part self-assembles at the core and the hydrophilic part turns towards their surface (Tian et al., 2017). Polar organic solvents that have the ability to dissolve lignin via breaking the inter and intramolecular bonds (Kai et al., 2015), are used in order to produce a lignin solution which is added (dropwise, dialysis) to an antisolvent (water) for precipitation in a controlled manner (Tian et al., 2017). Water is normally used as an antisolvent, owing to its low solubility for lignin (Schneider et al., 2021). The formation of LNPs occurs "in a hydrophilic aggregation by non-covalent interactions" such as hydrogen-bonds with the hydroxyl groups in the surface (Schneider et al., 2021; Tian et al., 2017), and tends to form spherical

nanoparticles to minimize the surface area contact with the antisolvent (Österberg et al., 2020).

Other non-covalent interactions such as van der Waals interactions of the organic solvent and π-π stacking of the aromatic compounds of lignin are also considered to the hydrophobic effect as they might cause aggregation (Deng et al., 2011; Qian et al., 2014; Sarkanen et al., 1982). Aggregation of lignin occurs through competition between electronic interactions (mainly aromatic compounds), repulsion force, and intermolecular H-bonds according to (W. Zhao et al., 2017). The aggregation process of LNPs is dependent on the concentration of organic solvent, antisolvent and the molecular size of lignin fragments. In case of an acetone-water mixture as organic solvent and water as antisolvent, the acetone concentration and water concentration (antisolvent) are the decisive factors for the formation of LNPs. A decrease of particle size with ascending antisolvent dilution rate up to a certain maximum was observed by Richter et al. (Richter et al., 2016) using highly hydrophobic and sulfur free high purity lignin (deriving from organosolv process) in acetone. It was assumed that beyond the threshold value of rapid mixing, the quantity of nuclei occurred has reached a maximum and no new nuclei were formed. It can therefore be concluded, that self-assembly proceeds from low to high molecular weight when adding diluted lignin to antisolvent, due to the ascending presence of nanoparticles and simultaneous decrease of antisolvent. Furthermore, a "kinetically controlled nucleation-growth mechanism" is initiated after a certain maximum of nuclei. In addition, interlinked networks as clusters and aggregates can occur if the assemble conditions are not controlled or the lignin concentration is too high (Österberg et al., 2020; Schneider et al., 2021; Sipponen et al., 2018).

The size of LNPs is also connected with the pH as they become smaller with increasing pH. The presence of aromatic functional groups on the surface leads to deprotonation and to a rise of surface charge, hence they get electrically stabilized at an earlier stage during nucleation growth mechanism (Österberg et al., 2020)

Naturally, the isolation method of lignin plays a vital role for the resulting properties of LNPs. For alkali lignin, such as kraft lignin or commercial Indulin AT, the amount of phenolic groups is high enough to not enable the development of dense packing in sphere-shaped nanoparticles due to electrostatic repulsion. Furthermore, the distinct hydrogen bonding between lignin and water hinders formation of colloids (Qian et al., 2014; Schneider et al., 2021). Therefore, chemical modification for alkali lignin such

as acetylation is necessary in order to enhance its hydrophobicity. Consequently, NPs with higher stability, better regular shape and smaller particle size can be achieved (Qian et al., 2014; Tian et al., 2017; Zhao et al., 2016).

Closely related to acetylation, esterification of lignin with citric acid and subsequent nanoparticle synthesis showed an improved dispersion in polar solvents and increase of thermal stability according to (He et al., 2018). Moreover, composites with antimicrobial properties could be achieved after forming LNPs from esterified tall oil fatty acids (Setälä et al., 2020).

2 Objectives

The aim of this study is to implement selective esterification methods for kraft lignin in order to achieve value-added products in a sustainable manner.

A recently published mild acetylation method for cellulose without heating was adapted to kraft lignin using *N*-acetylimidazole as reactant solely (Beaumont et al. 2021, Beaumont et al. 2020). Considering the advantages of the method, such as mild and energy-efficient conditions, its adjustment to lignin modification would provide a novel sustainable and straight-forward approach to tune lignin properties and to expand its value-added applications. Therefore, the development of the solid-solid reaction with kraft lignin and *N*-acetylimidazole was examined and optimized with a design of experiment (DoE). The influence of moisture content, amount of *N*-acetylimidazole and reaction time on the degree of substitution (DS) was studied.

To increase the versatility of this modification, a solvent-free reaction with carboxylic acid anhydrides and imidazole (Im) was optimized to introduce esters with varying size and length. Based on this approach acetylated lignin as well as isobutyric and hexanoic lignin esters of different DSs were produced. These functional lignins were used to prepare nanoparticles and further implemented to study the influence of functional group and DS on the particle formation. The influence of these factors on wettability, surface tension, morphology, colloidal stability and size of the nanoparticles was studied.

3 Results and discussion

With the objective of transferring the principle of acetylation with *N*-acetylimidazole from cellulose to kraft lignin as a mild, solvent free, solid-solid reaction, the lignin had to be treated beforehand. Beaumont et al. (Beaumont et al., 2021) showed that water promotes surface reactions of nanoporous polymeric structures.

Therefore, the compatibility of the reaction to lignin was tested in moist condition as well (9.9% moisture content). A qualitative conversion was confirmed on the basis of methyl signals in ^{1}H-nuclear magnetic resonance (^{1}H-NMR) and a carbonyl band through Fourier transformed infrared spectroscopy (FTIR) measurement. As soon as the first proof of concept was performed, systematic experiments were carried out. A quantitative method for the DS (synonymously degree of acetylation/esterification) was established (3.1) in order to study the reaction parameters and optimize them (3.3.1). In general, Indulin was mixed thorough with water to reach different moisture contents. Variations in reaction times were realized by 30 min sample milling followed by remaining resting time for complete conversion. The DS for lignin was calculated as the number of substituent groups (acetyl/ester group) replaced per total amount of hydroxyl groups. The concept of solvent free acetylation was extended, first to acetylation with acetic anhydride (AA) and Im as catalyst (3.2), followed by optimization of the parameters (3.3.2), and esterification with different carboxylic acid anhydrides (3.4). Thereby, a set of lignins with different functional groups and DSs were produced. These modified lignins were characterized by NMR and FTIR to study their functionalization degree. The esterified lignins were used to prepare nanoparticles (3.5.1), which were studied in detail using dynamic light scattering (DLS) and atomic force measurements (AFM) for particle size and morphology analysis (3.5.2, 3.5.3). The physical properties of the nanoparticles were further examined by ultraviolet-visible spectroscopy (UV-VIS), goniometry, electrophoretic analysis and pendant drop measurements (0-3.5.8).

3.1 Acetylation of lignin with *N*-acetylimidazole

3.1.1 Proof of concept

The reaction of *N*-acetylimidazole with commercial kraft lignin (Indulin AT) was carried out in a ball mill. This method was chosen because it offers mild efficient mixing and instant start of reaction with no need of solvent (Beaumont et al., 2021).

For solvent-free acetylation, Indulin AT (9.9% moisture content) and *N*-acetylimidazole were mixed in a ball mill. Reaction was quenched by an addition of DI water yielding acetic acid (AcOH) and Im as by-products. Qualitative conversion was examined using FTIR (Figure 6) and ^{1}H-NMR (Figure 7) analysis.
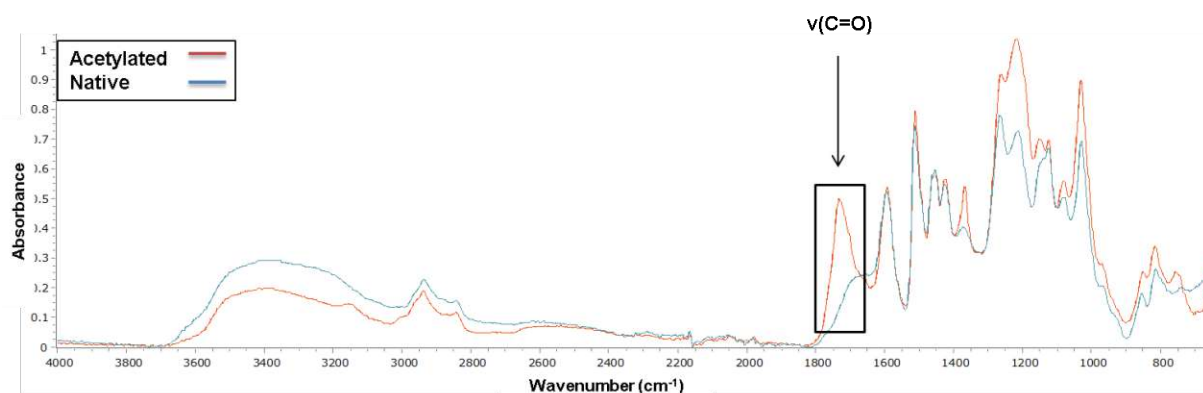
Figure 6: FTIR spectra of acetylated Indulin AT in comparison to the starting material (native).
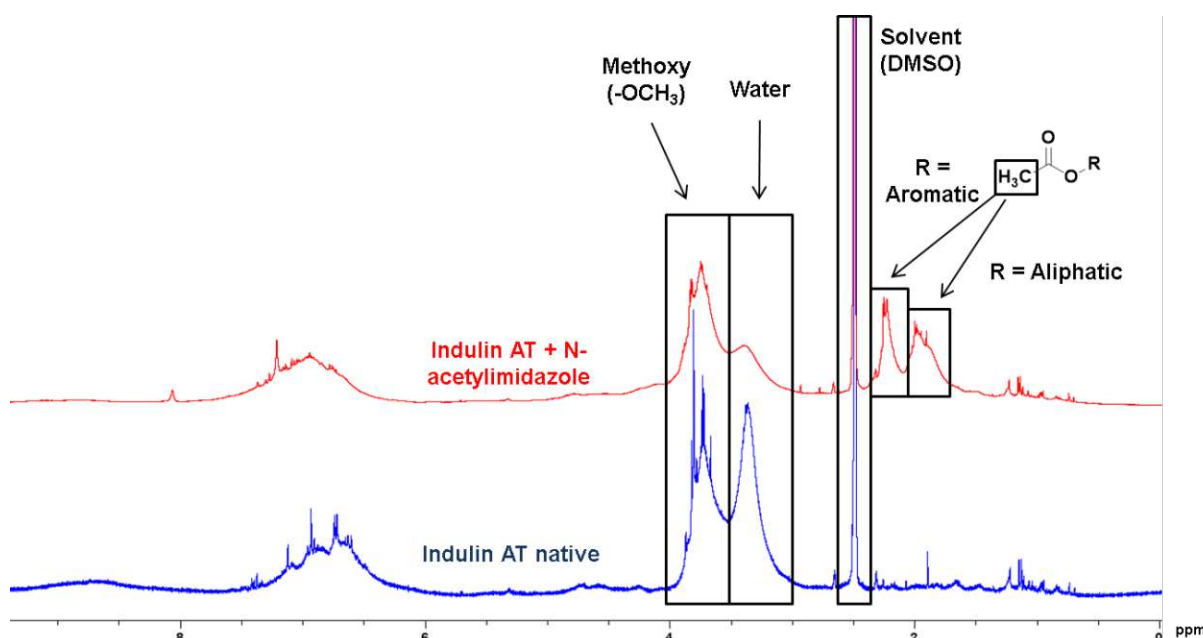
Figure 7: ^{1}H-NMR spectra of acetylated Indulin AT in comparison to the starting material (native).

The carbonyl band (v(C=O)) at 1730 cm^{-1} in Figure 6 indicates conversion to acetylated lignin. In Figure 7, it is clearly shown through the presence of the proton peaks corresponding to the acetyl group that the modification was successful. Therefore, this simple and convenient method provides a one-step acetylation synthesis without a usually necessary drying step, since typical esterification reactions have mainly been performed under anhydrous conditions due to the competition of hydroxyl groups on the surface of lignin (Glasser and Jain, 1993; Lewis et al., 1943). Furthermore no continuous energy supply in the form of milling or

heating in contrast to other (mechano)chemical esterification processes was necessary (He et al. 2018; Thielemans and Wool 2005; X. Zhao et al. 2017). In the method developed herein, the ball mill treatment is just necessary to mix the reactants, as the reaction of the lignin hydroxyl groups and the *N*-acetylimidazole is spontaneous, which makes the reaction more sustainable and energy efficient.

3.1.2 Determination of DS

The reaction was optimized with a DoE by systematically analyzing the influence of the following factors: moisture content, reaction time and amount *N*-acetylimidazole. In total 26 runs were conducted. With the purpose of determining the efficiency, the highlighted peaks in Figure 7 were used to estimate the DS. The integrals of the peaks corresponding to the acetyl groups were related to the ones of the methoxy groups (which should be unaffected by the chemical modification). Based on the chemical shift, the substitution at aliphatic and aromatic groups can be distinguished. In order to achieve the best possible comparability, the peak ranges for the integrations were kept constant for all 26 runs (see Table 1).

Table 1: ^{1}H-NMR ranges set for functional groups.

Range ^{1}H-NMR (ppm)	Functional groups
4.164-3.505	methoxy
2.414-2.079	acetyl aromatic
2.079-1.601	acetyl aliphatic

Based on the NMR results, the DS was estimated in relation to the total amount of methoxyl groups in the unmodified Indulin sample.

However, this method gives just the relative DS of the sample, and needs to be calibrated with a quantitative method, such as the phosphorus method. A phosphorus-containing reagent (phospholane) induces derivatization of the free hydroxyl groups which is subsequently analyzed using ^{31}P-NMR measurement and compared to a native sample. It was chosen as a straight forward method according to Argyropoulos (Argyropoulos, 1994). In total, 13 samples were measured to build up a calibration curve. The peaks of the aliphatic and aromatic methyl groups and their corresponding ppm ranges used for the analysis are shown in Figure 8.

Range ^{31}P-NMR (ppm)	Hydroxyl derivatization
150-144.6	aliphatic
144.6-137	aromatic
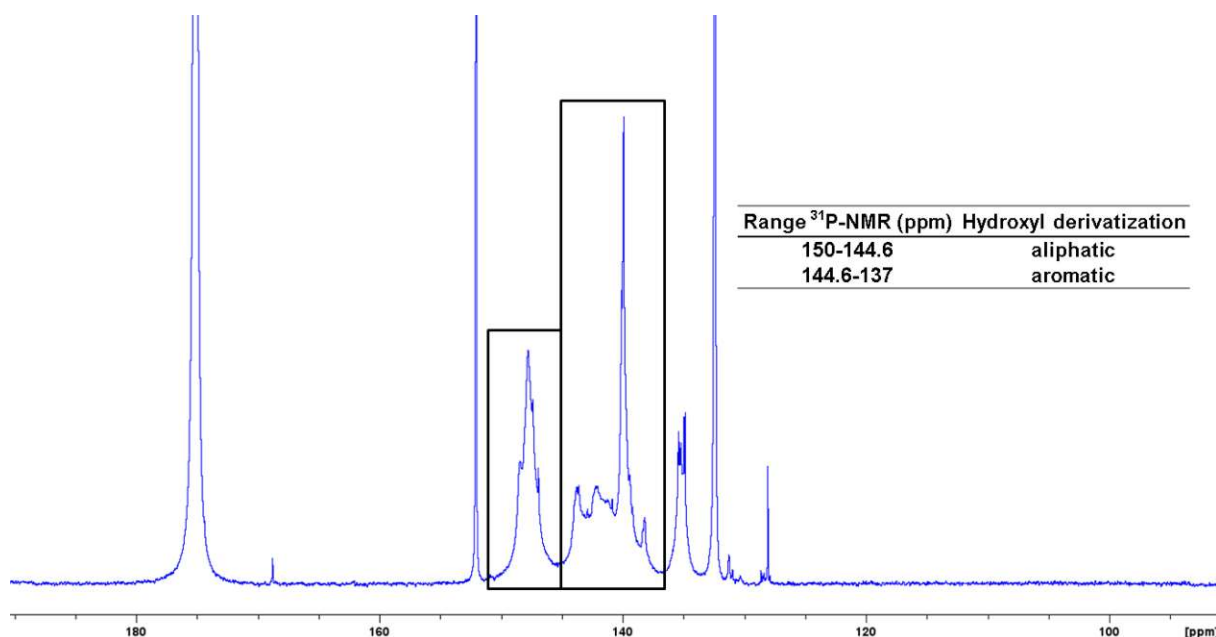
Figure 8: Example of ^{31}P-NMR spectra with ranges for aromatic and aliphatic signals of phospholane derivatization at free hydroxyl lignin groups.

The integrals of these two signals related with the internal standard (12.52% methoxy groups) were used to calculate the amounts of remaining, unmodified hydroxyl groups. The lower the amount of remaining hydroxyl groups (in relation to the total amount of hydroxyl groups, 6.52 mmol/g), the higher the DS.

By plotting the DS determined with the phosphorus method against the relative degree of substitution (rel. DS) determined via ^{1}H-NMR, the calibration curve in Figure 9 was constructed.
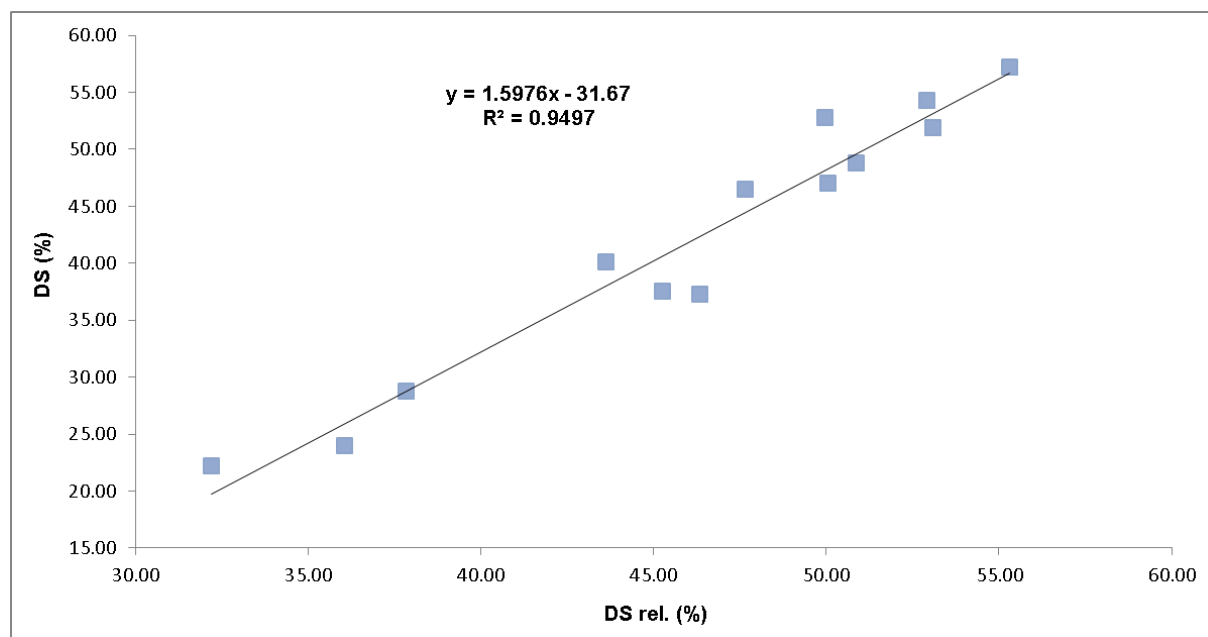
Figure 9: Calibration curve to enable quantitative analysis of the DS with simple ^{1}H-NMR analyses. The relative DS values from ^{1}H-NMR spectroscopy were calibrated with DS values obtained via phosphorylation and ^{31}P-NMR analysis (phosphorus method).

The calibration curve had a R^2 value of 0.95, which is an adequate result considering the heterogeneity of the used Indulin AT sample. The developed calibration curve facilitates the determination of the DS of the modified lignins by implementing a fast and simple ^{1}H-NMR analysis, which does not require any previous derivatization as in case of the phosphorus method.

3.1.3 Reaction optimization

The performed experiments for the DoE are listed in Table 2. The DS was used as response value for further analysis.

Table 2: Conducted experiments for the DoE (reaction time (h), moisture content (wt%) and *N*-acetylimidazole (eq)) with DSs (%).

Run	*N*-acetylimidazole (eq.)	Moisture content (wt%)	Reaction time (h)	DS (%)
1	0.55	24.60	2.47	42.38
2	0.74	17.30	1.75	53.67
3	0.48	9.90	1.03	34.85
4	0.91	9.90	1.03	49.57
5	0.74	17.25	1.75	52.60
6	1.15	17.25	1.75	56.69
7	0.74	17.25	3.00	48.09
8	0.34	17.25	1.75	25.95
9	0.55	24.60	1.03	37.03
10	0.74	17.25	1.75	48.87
11	0.91	9.90	2.47	53.14
12	0.83	30.00	1.75	48.30
13	1.03	24.60	2.47	48.15
14	0.48	9.90	2.47	36.57
15	0.74	17.25	1.75	50.96
16	0.74	17.25	0.50	40.63
17	0.64	4.50	1.75	38.00
18	1.03	24.60	1.03	57.33
19	0.74	17.25	1.75	48.62
20	0.64	4.50	1.75	28.76
21	0.83	30.00	1.75	44.22
22	0.74	17.25	1.75	44.45
23	0.74	17.25	0.50	43.25
24	1.15	17.25	1.75	52.84
25	0.74	17.25	3.00	45.70
26	0.34	17.25	1.75	19.76

In Table 2, the DS of the acetylation reaction is listed under varying conditions. The highest DS could be achieved in run 18 (57.33%). Other acetylation methods of kraft lignin using for example AA, pyridine (as catalyst) and microwave assistance (Monteil-Rivera and Paquet, 2015) or AA in choline chloride (both at varying temperatures and reaction times) (Li et al., 2020) achieved a DS of above 95%. In

contrast, this mild method selectively modifies the chemically most accessible groups since the reaction is heterogeneous and not conducted in solution. Previous studies showed that *N*-acetylimidazole executes rather an acetyl transfer than a traditional esterification ("which would be subject to the law of mass action and thus not work in aqueous medium") owing to its specific structure (Abushammala et al., 2017; Beaumont et al., 2020; Zweckmair et al., 2015). Competing interactions inside the lignin structure, such as H-bonds, inhibit the reachability of hydroxyls. Thus, lower DSs were achieved. The water also affects the DS as it was reported to reduce the activation energy (similar to a catalyst) and increases the reaction rate and efficiency during acetylation processes (Beaumont et al., 2021).

The optimal moisture content and reaction time of the lignin acetylation with *N*-acetylimidazole was determined in Chapter 3.3.1 based on the results in Table 2.

3.2 Acetylation of lignin via *in situ* preparation of *N*-acetylimidazole

3.2.1 Reaction mechanism

An additional pathway to synthesize acetylated lignin in a solvent-free and mild reaction is the *in situ* preparation of *N*-acetylimidazole followed by its reaction with lignin. This method and the previously described acetylation approach carried in a ball mill are schematically described in Scheme 1.
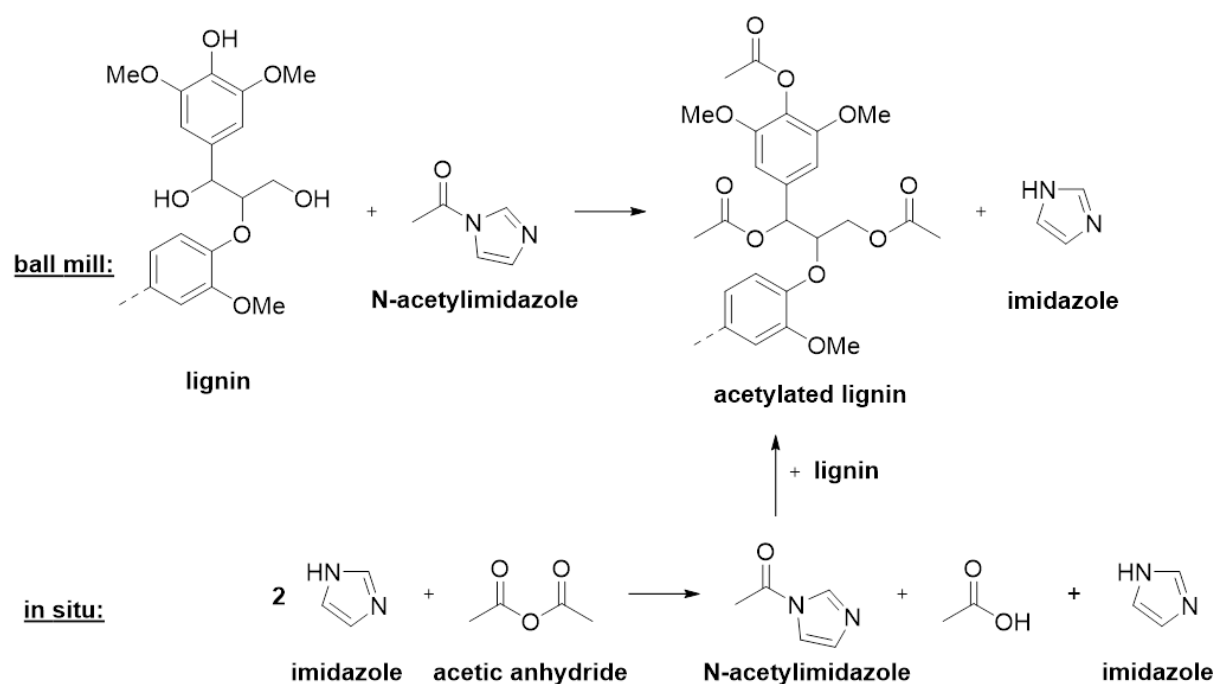
Scheme 1: methods for acetylated lignin: lignin and *N*-acetylimidazole in a direct solid-solid reaction with a ball mill and *in situ* preparation of *N*-acetylimidazole with Im and acetic anhydride followed by its reaction with lignin.

In Scheme 1 the acetylation pathways obtaining acetylated lignin are compared. Im was chosen as catalyst because of its enzyme-like catalytic behavior and structural analogy to histidine (Nothling et al., 2017). Both are solvent free reaction but the pathway for *in situ* acetylation offers more flexibility in contrast to the process in the ball mill, as different esters with, e.g., variable alkyl chain lengths can be introduced by substitution of AA with other anhydrides. *N*-acetylimidazole, which is used in the ball mill process, is also less stable compared to anhydrides, hence the *in situ* production tackles the issue of limited storage stability of the reactants.

3.2.2 Reaction optimization

Indulin AT, AA and Im were mixed together in that particular sequence because pre-experiments showed that an inhomogeneous and highly viscous mixture was obtained when Indulin and Im (both are solids) were first mixed and AA (liquid) was added subsequently. In total, 12 experiments were carried out in a DoE. Since the principle reaction mechanism is the same as for the ball mill approach (see 3.3.1), we used the optimized moisture content and reaction time from the first reaction for the anhydride/Im approach.

Different ratios of AA and Im were tested during reaction optimization (see 3.3.2). The minimum of AA was set to 0.78 eq (a lower amount of AA resulted in an inhomogeneous mixture). Im was added varying from equimolar to three equivalents. Two equivalents are intended for reaction with AA for the synthesis of *N*-acetylimidazole and forming an imidazolium acetate salt as shown in Scheme 1. Equimolar addition of Im leads to the formation of *N*-acetylimidazole and AcOH, and an excess of Im results in *N*-acetylimidazole, imidazolium salt and remaining Im. Hence, the presence of either salt, free Im or AA is expected to influence the reaction efficiency.

The equivalents of AA and Im with corresponding DS (evaluated with the calibration curve from Figure 9) are listed in Table 3

Table 3: Investigated factors in the DoE (AA (eq), ratio of AA (eq) to Im (eq)) and their DS (%). A moisture content of 17.25% and a reaction time of 2 h were kept constant in all experiments.

Run	AA (eq)	AA (eq) / Im (eq)	DS (%)
1	1.17	2.00	68.61
2	1.45	2.71	77.53
3	1.17	1.00	74.57
4	1.17	2.00	62.87
5	1.17	2.00	58.19

6	1.56	2.00	80.12
7	1.17	2.00	62.79
8	0.90	2.71	53.86
9	1.45	1.29	75.64
10	0.78	2.00	44.79
11	0.90	1.29	47.52
12	1.17	3.00	64.10

Table 3 shows that highest DS of 80.12% was achieved through lignin acetylation with AA and Im. Therefore, the maximum DS is 23% higher than the one for ball milling acetylation. This can be reasoned by a higher accessibility of hydroxyls in a liquid dispersion of reagents due to the utilization of liquid anhydride. Moreover, partial dissolution of lignin could have occurred in the reactant.

The DS of both optimized reactions were further graphically analyzed by means of a box plot diagram.
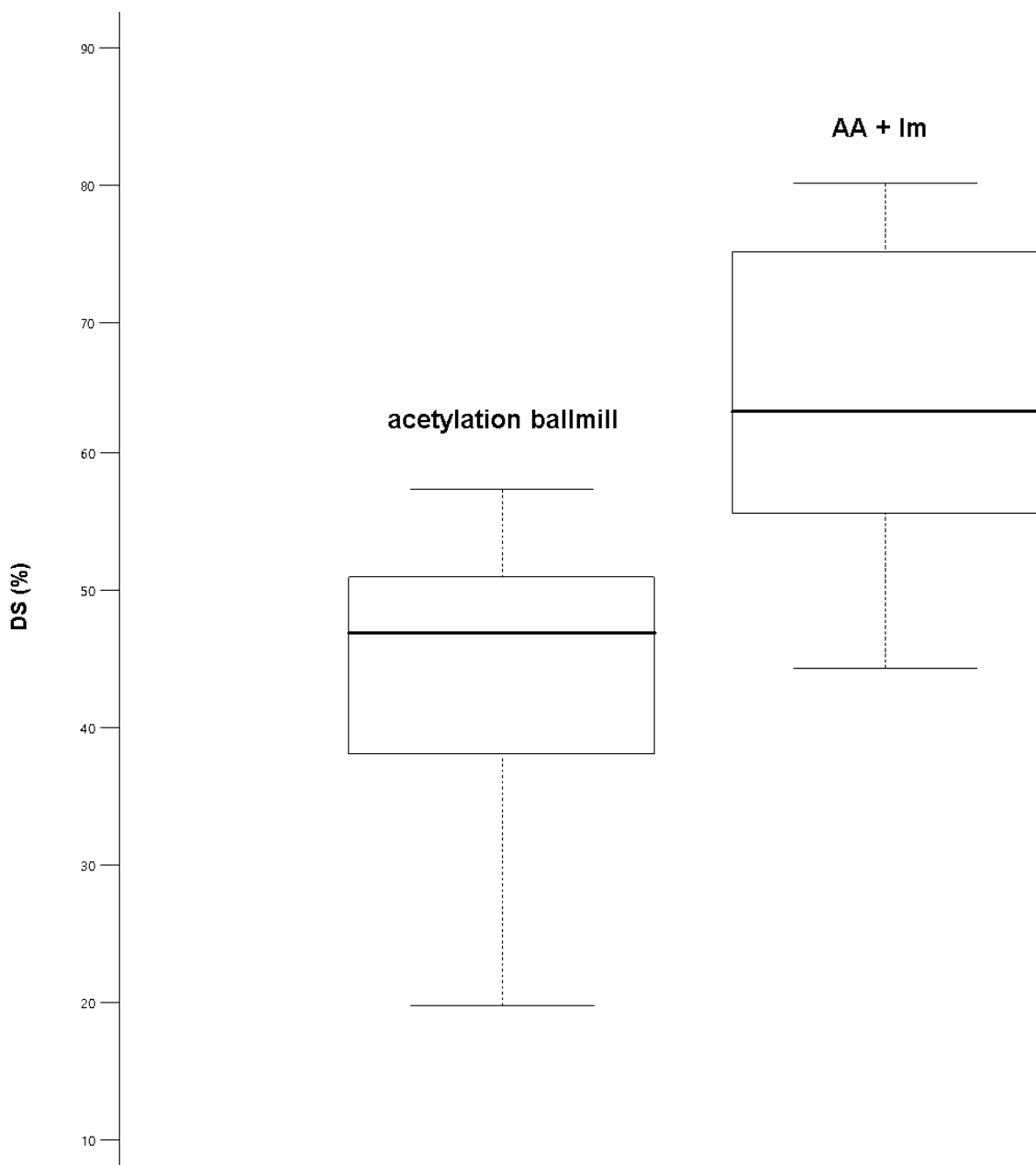
Figure 10: Box plot for DS (%) of acetylated lignin via ball mill (left) and acetylated lignin via AA and Im (right). The figure includes all reactions performed with each type of procedure to visualize the accessible DS range of acetylated lignins.

In Figure 10 the distribution of DSs obtained for both lignin acetylation methods is shown graphically. The DS is located between 22.75% to 58.66% for the ball mill method and 56.02% and 80.12% when using AA and Im. The respective medians are marked with a bright horizontal line and account for 47.87% (ball mill) and 63.49% (AA + Im). Hence a 15.62% higher DS on average could be achieved for the *in situ* method due to improved accessibility of the lignin hydroxyl groups. One has to keep in mind that in case of the ball mill method, different moisture contents and reactions times were tested, whereas the optimized values of both were used for the reaction using AA and Im, reasoning partially the difference in average DS values.

30

Interestingly, the ball mill method shows a slightly higher product recovery after calculating the theoretical yield (with regard to 6.52 mmol/g hydroxyl groups of native indulin) achieving 87.64% (see Table 21) comparing to 80.38% (see Table 24) on average for the in situ method (for all runs performed respectively). Both methods provide adequate mass yields considering that the work-up is performed by repeated aqueous washing steps followed by centrifugation, and subsequent decantation.

3.3 Optimization of lignin acetylation methods

For acetylation of lignin with *N*-acetylimidazole (3.1) as well as for acetylation of lignin via *in situ* preparation of *N*-acetylimidazole (3.2) an in-depth analysis as DoE was executed in order to determine the optimal reaction parameters.

3.3.1 Design of experiment for acetylation of lignin with *N*-acetylimidazole

Centered on the study of Beaumont et al. (Beaumont et al., 2021) suggesting that higher moisture content of cellulose improves acetylation reaction rates and efficiency, the Indulin moisture content and the total reaction time (30 min milling were kept constant and the resting time was varied) were used as varying parameters. The amount of *N*-acetylimidazole (limiting reactant) was set as varying parameter too, to check weather a saturation of acetylated lignin occurs at certain point. Preliminary experiments showed no significant influence on the DS when varying the amount of steel balls during ball mill synthesis. Thus, this factor was kept constant.

A model, including 4 central points and 9 factorial points with two replications (26 runs) was designed. The DS was defined as response (R1) and the corresponding values are listed in Table 2. With the aim of achieving the best reaction conditions more information had to be generated, starting with setting a fit for the response.

Table 4: Fit summary for acetylation of lignin with *N*-acetylimidazole.

Source	Sequential p-value	Lack of Fit p-value	Adjusted R²	Predicted R²	
Linear	< 0.0001	0.02	0.71	0.66	
2FI	0.42	0.02	0.71	0.63	
Quadratic	0.00	0.18	0.83	0.67	**Suggested**
Cubic	0.18		0.87		**Aliased**

The DoE software automatically evaluates the best fit for certain investigation (Table 4) which in this case suggested a quadratic fit with a rounded adjusted coefficient of determination (R^2) of 0.83. Sequential p-value and Lack of Fit p-value are not

significant for the quadratic fit. The cubic fit would have had a marginal higher adjusted R^2 value but was aliased due to a significant lack of fit.

Furthermore an ANOVA (analysis of variance) was compiled (see Table 5).

Table 5: Analysis of variance of the quadratic fit for acetylation of lignin via *N*-acetylimidazole.

Source	Sum of Squares	Mean Square	F-value	p-value
Model	2231.690	247.970	15.940	< 0.0001
A-Moisture content	14.060	14.060	0.904	0.354
B-*N*-Acetylimidazole	1607.340	1607.340	103.300	< 0.0001
C-Reaction time	36.960	36.960	2.380	0.141
AB	0.226	0.226	0.015	0.905
AC	5.000	5.000	0.321	0.578
BC	21.560	21.560	1.390	0.255
A²	123.690	123.690	7.950	0.011
B²	263.160	263.160	16.910	0.001
C²	44.610	44.610	2.870	0.108

The ANOVA illustrates the F-values and p-values as well as the sum of squares and mean square for all 3 factors and their combinations detailed in Table 5. The higher the F-value the more significant the factor. P-values less than 0.05 indicate significance of the model and values above 0.1 are not significant.

Applied on the ball mill method, the model itself is significant which is important when compiling a model for a specific task. The amount of *N*-acetylimidazole (factor B) is distinctly the factor with highest impact on the DS, showing the lowest p-value and highest F-value. Moisture content and reaction time (factors A and C) have certain influence on the efficiency of the reaction but not significant according to p-value and F-values in Table 5. Interestingly, the p-value of A^2 (moisture content) is below 0.05 (0.011) and thus moisture content influences the DS. In contrast, the reaction time offers no combination (C, AC, BC, C^2) obtaining a p-value below 0.05. Hence, lignin acetylation using a ball mill is independent of the reaction time and consequently this factor is excluded for further optimization analysis.

A 3D- diagram plotting the DS against the two remaining factors was designed summarizing the whole DoE (see Figure 11).
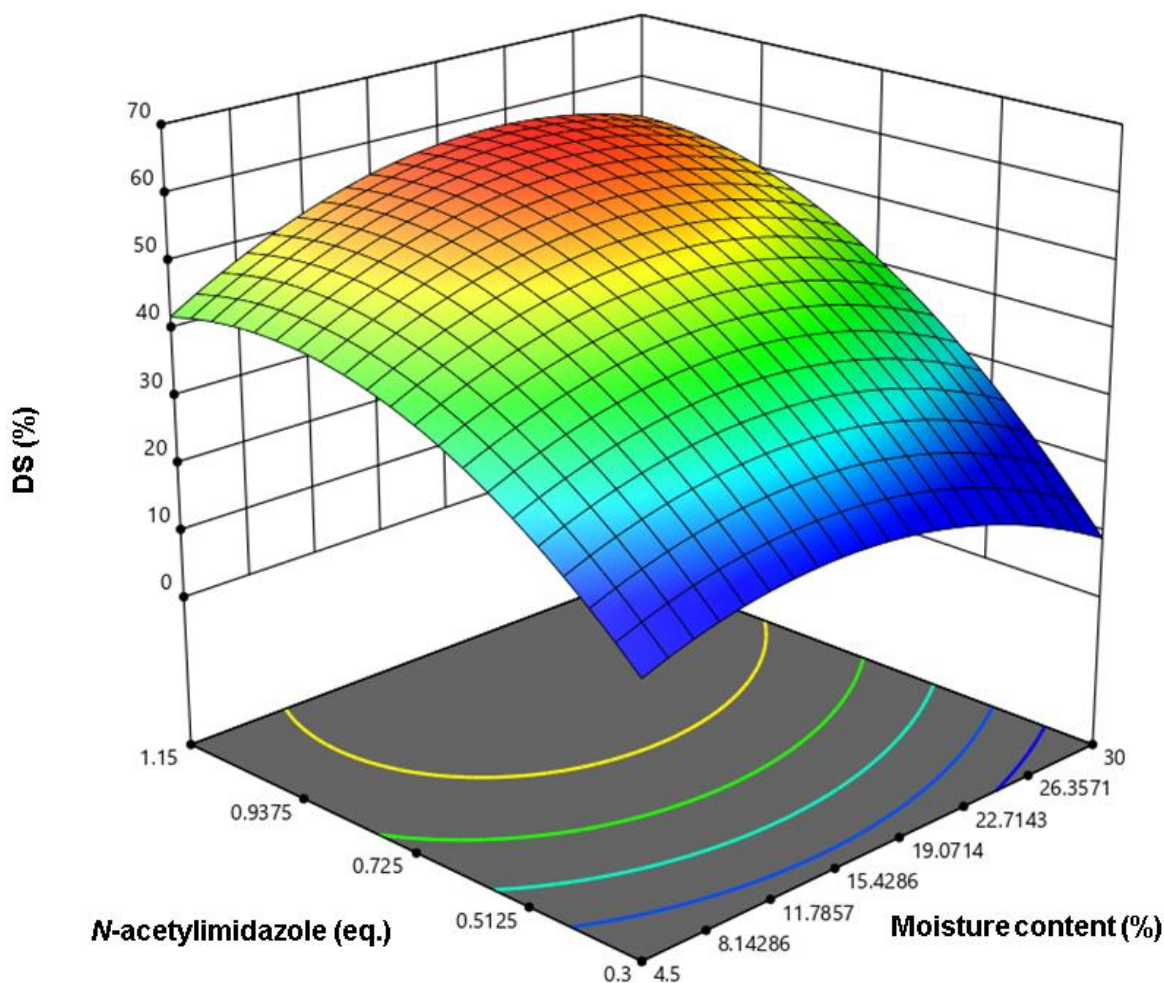
Figure 11: 3D- diagram from the DS against *N*-acetylimidazole and moisture content.

The significant data of the performed 26 runs are collected in Figure 11 accentuated from red to blue for samples with high to low DS, respectively (the response R1 is the DS of the respective sample).

Considering the *N*-acetylimidazole content: a direct proportionality is identified starting with a high linear increase and switching to a plateau as of about 0.95 eq. The second-order fit describes the influence of moisture content on the reaction yield with the maximum observed at 17.25%. It can be concluded that acetylation is slightly favored up to a certain point of moisture content. The lower efficiency at higher moisture content is most probably reasoned by a lower stability of the acetylation agent *N*-acetylimidazole, or by a competing hydrolysis of the introduced acetyl groups.

However, highest conversions should therefore be achieved at a moisture content of 17.25% and 1.15 eq of *N*-acetylimidazole (see red area in Figure 11). Reactions at these conditions were carried out twice to validate the data reproducibility.

Table 6: Validation experiments with optimized conditions.

Run	N-acetylimidazole (eq.)	Moisture content (%)	Reaction time (h)	DS (%)
27	1.15	17.25	1.87	53.01
28	1.15	17.25	1.87	57.16

Both DS values of the validation are in a comparable range (compare Table 2) showing a reasonable data reproducibility.

3.3.2 Design of experiment for Acetylation of lignin via *in situ* preparation of *N*-acetylimidazole

As described above, the optimal conditions were determined for lignin acetylation. Therefore, the moisture content (17.25%) and reaction time (2 h) were kept constant for the *in situ* acetylation method. Even though the reaction time showed no significant influence on the DS for the ball mill method, it was set to 2 h for *in situ* method in order to allow complete conversion. Most influence on the DS was determined for *N*-acetylimidazole, the acetylation agent. Because it is produced *in situ* using AA and Im (Scheme 1) those factors were set as varying factors. Based on the fact that the highest amounts of acetylation agent (1.15 eq) results in a highest DS, the amounts for AA were chosen right above and below this value (0.78 – 1.56 eq, see Table 22). The amount of Im was set in a broad range in order to study its influence on acetylation (cf. 3.2, see Table 22).

For DoE study, the response (DS) was evaluated by setting an appropriate fit.

Table 7: Fit summery for acetylation of Indulin with AA.

| Source	Sequential p-value	Lack of Fit p-value	Adjusted R^2	Predicted R^2	
Linear	< 0.0001	0.35	0.84	0.75	**Suggested**
2FI	0.66	0.32	0.83	0.68	
Quadratic	0.35	0.31	0.84	0.57	
Cubic	0.19	0.44	0.92		**Aliased**

A quadratic fit was suggested to be the best fit for certain DoE indicated in Table 7. The R^2 is 0.84 (second highest) for the linear fit and sequential p-value below 0.0001 substantiates the choice. The cubic fit would have had a higher adjusted R^2 value but was aliased by the software.

An ANOVA (analysis of variance) was compiled with a focus on statistical information (see Table 8).

Table 8: Analysis of variance of the linear fit for acetylation of Indulin with AA.

Source	Sum of Squares	Mean Square	F-value	p-value
Model	1300.86	650.43	30.84	< 0.0001
A-1-AA	1295.44	1295.44	61.42	< 0.0001
B-1-AA / Im	5.41	5.41	0.26	0.62

The sum of squares, mean square F-values and p-values were evaluated as ANOVA and listed in Table 8. The model exhibits significance for the adjusted linear fit. Lower p-values values than 0.05 and the highest F-value are determined for AA (factor A). This represents a significance of factor A on the DS, whereas the ratio of AA to Im shows p-value than 0.1 resulting in no significance. Hence the mass of Im is not dependent on the response in the investigated range. Therefore, factor B is not considered for further evaluation (cf. reaction time (3.3.1)). A graphical dependence of the remaining factor (amount of AA) can be seen in Figure 12.
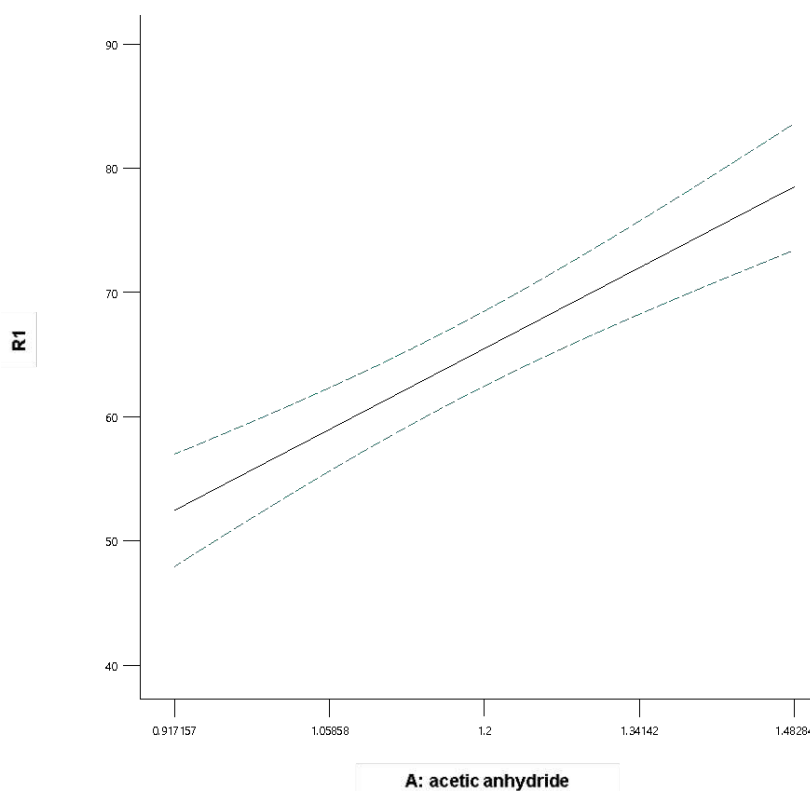
Figure 12 : DS (%) against AA (eq).

In Figure 12 a direct linear dependency of AA to the DS with confidence bands is pictured for the investigated range. All other compiled data are in accordance to the curve progression which thus summarizes the whole DoE (see above).

The following optimal conditions for solvent-free acetylation of indulin using AA and Im (without continuous energy supply) have been determined: lignin moisture content

of 17.25% and addition of 1.56 eq AA. A reaction time of 2 h and the addition of 2 eq. Im are further recommended.

3.4 Esterification of lignin via *in situ* preparation of *N*-acylimidazole

The concept of lignin acetylation via *in situ* preparation of *N*-acetylimidazole (3.3) was extended to introduce different ester groups.
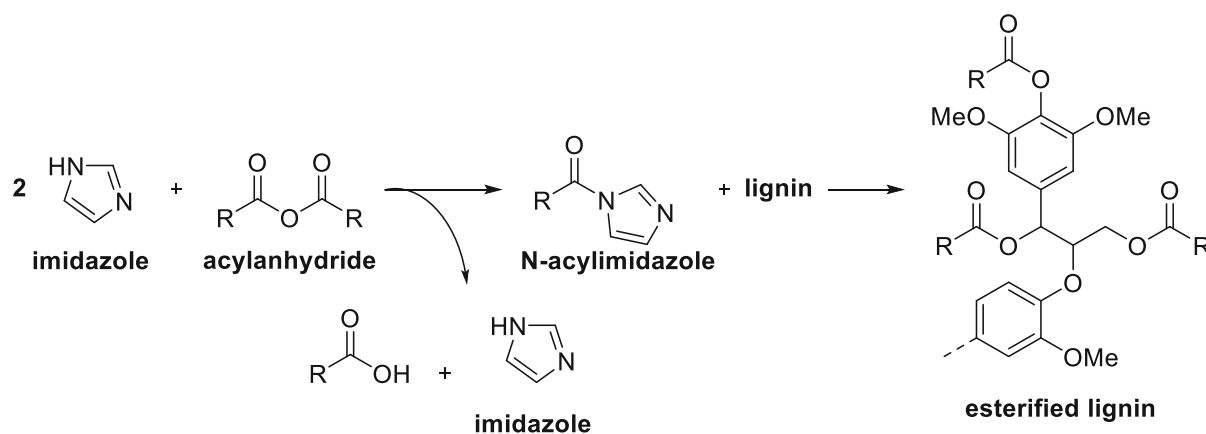
Scheme 2: Reaction of lignin with *in situ* prepared *N*-acylimidazole yielding lignin esters and R=alkyl.

This method allows a great versatility in fabrication of lignin esters. In general, the length and the size of introduced alkyl group (R) influences the chemical properties of synthesized lignin ester. Hence, in this thesis an n-alkyl group and more bulky alkyl groups, precisely, n-hexyl and isobutyl were selected. Furthermore, based on the optimization of acetylation syntheses, a medium (M), high (H) and very high (HH) DS for the respective lignin esters were generated selectively. The influence of the parameters on the DS was therefore adapted for M and H DSs. Very high DSs were achieved through synthesis procedure according to (Thielemans and Wool, 2004) but replacing *N*-methylimidazole by Im.

3.4.1 Esterification of Lignin with isobutyric anhydride (IBA)

Syntheses were carried out under varying conditions in order to achieve isobutyric lignin esters with different DS. Considering that the DS is solely dependent on the amount of added anhydride (at constant moisture content) at least in case of acetylation in Chapter 3.2, we assume that the exact modification conditions using a different anhydride as a sole difference applied, will behave similarly. Thus, the AA equivalent amount that provided the highest DS in acetylation reaction (1.56 eq) was taken for isobutyric anhydride (IBA) with the expectation to achieve a high DS during esterification. To achieve a medium DS, a medium amount of the reagent (0.9 eq)

was taken. The respective values of Im were adopted as well (see run 6 & 8 Table 3). Isobutyric lignin esters with very high DS were synthesized using a large excess of IBA. The reaction mixture was heated to 50 °C for 18 h. The evaluation method had to be reconsidered because the aromatic and aliphatic protons overlapped in ^{1}H-NMR in contrast to acetylated lignins (cf. Figure 7). Therefore, distinguishing between aromatic and aliphatic OH was no longer possible, and thus the whole area was selected for determination of the total DS (see Figure 13).
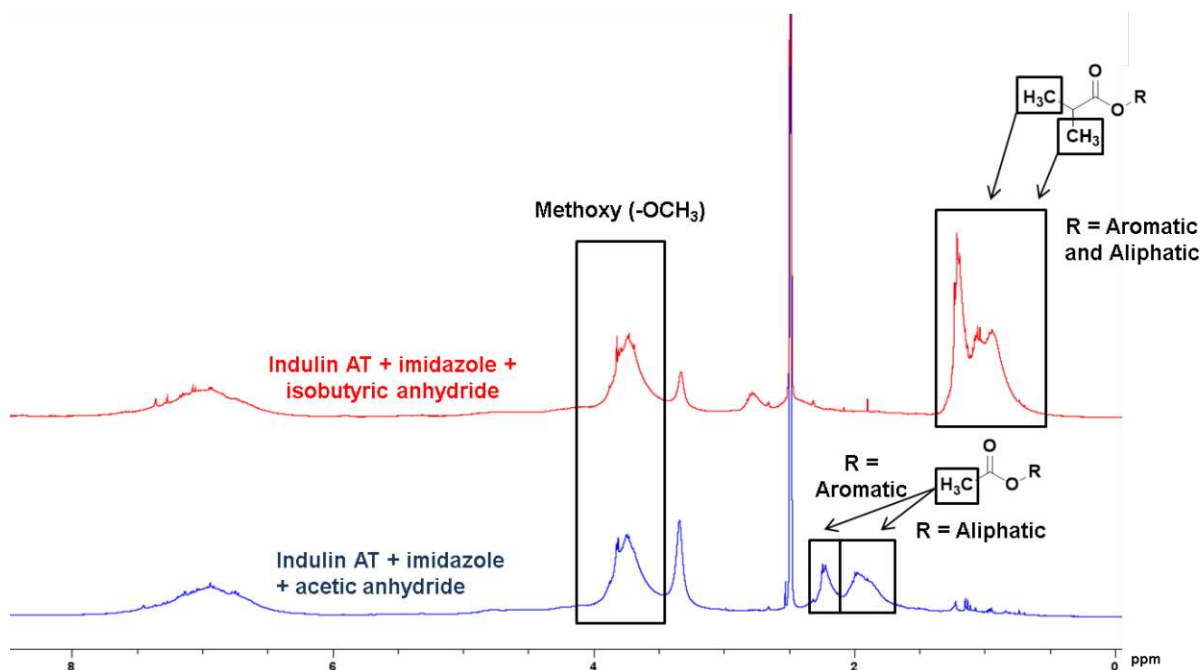
Figure 13: Example for ^{1}H-NMR spectra of butyric ester in comparison to acetic ester and the selected areas for the determination of the DS.

Examples for ^{1}H-NMR spectra of butyric and acetylated lignin ester respectively are shown in Figure 13. The marked regions of indistinguishable aromatic and aliphatic protons illustrate the ppm ranges which were used for the DS calculation and can be seen in Table 9.

Table 9: ^{1}H-NMR ranges for all isobutyric syntheses and corresponding functional groups.

range ^{1}H-NMR (ppm)	functional groups
4.03-3.503	methoxy
1.34-0.63	butyric

Evaluation of DS was conducted identically to the acetylation experiments (see 3.1) except that all six protons of the two methyl groups had to be taken into consideration. Obviously, the molar masses and moles were changed accordingly. The parameters and results are summarized in Table 10.

Table 10: Moisture content (%), reaction time (h), IBA (%), ratio of IBA (eq) to Im (eq) and DS (%) for isobutyric lignin esters.

IBA	Moisture content (%)	Reaction time (h)	IBA (eq)	IBA (eq) / Im (eq)	DS (%)
medium	17.25	2.00	0.90	1.29	66.65
high	17.25	2.00	1.56	2.00	93.46
very high	17.25	2.00	1.82	5.95	102.89

The DS obtained were correlating well with the reagent amount, providing the following results: 66.65% for medium (M), 93.46% for high (H) and 102.89% for very high (HH) amount of IBA (Table 10). Higher values than 100% are theoretically not possible but taking the selected area for all 6 acetyl protons and the proton on alpha position (signal at about 2.6 ppm) into consideration small deviations during peak integration occur quite easily. Still, the DS determined by ^{1}H-NMR (^{31}P-NMR) can be considered as powerful tool for data evaluation.

3.4.2 Esterification of lignin via hexanoic anhydride (HA)

Preparations of hexanoic lignin esters with M, H and HH DS were performed in analogue to those using IBA (3.4.1). The experimental procedures and the reagent amounts in moles were exactly the same with the exception that the modified samples needed a further purification step due to its reduced solubility in water caused by the presence of long non-polar hexyl groups in its structure. A minimum volume of pure acetone was added to the crude product to achieve its full dissolution. Subsequent precipitation in hexane completed the purification process. DS determination was carried out based on ^{1}H-NMR measurements (see Figure 14).
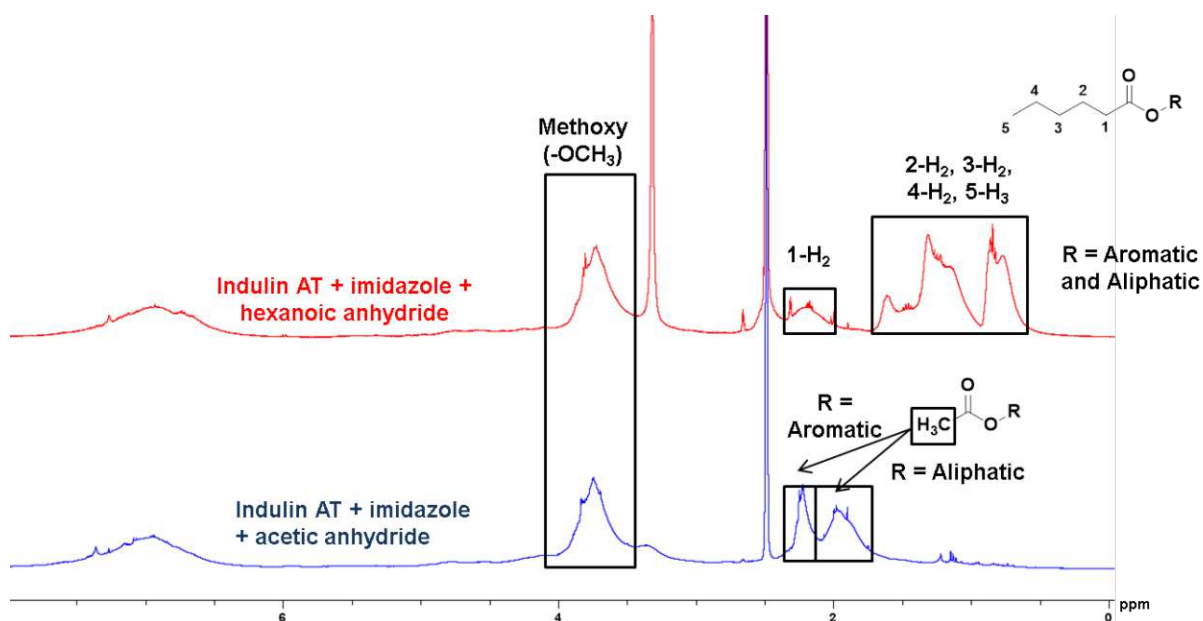
Figure 14: Example for ^{1}H-NMR spectra of hexanoic ester in comparison to acetic ester and the selected areas for DS determination.

In Figure 14 the ^{1}H-NMR spectra for hexanoic and acetic lignin esters, as well as the selected areas for DS determination are shown. Alike butyric lignin esters, the signals are indistinguishable for hexanoic lignin esters and the ppm ranges for ^{1}H-NMR analysis are listed in Figure 14.

Table 11: ^{1}H-NMR ranges for all hexanoic syntheses and corresponding functional groups.

range ^{1}H-NMR (ppm)	functional groups
4.022-3.494	methoxy
1.725-0.544	hexanoic

DS determination was carried out similar to isobutyric esters. The whole area of hydrocarbons (9 protons in total) had to be considered for analysis. Molar masses and moles were adapted with the aim of calculating the DSs (see Table 12).

Table 12: Moisture content (%), reaction time (h), HA (%), ratio of hexanoic anhydride (eq) to Im (eq) and DS (%) for hexanoic lignin esters.

HA	Moisture content (%)	Reaction time (h)	HA (eq)	HA (eq) / Im (eq)	DS (%)
medium	17.25	2.00	0.90	1.29	47.84
high	17.25	2.00	1.56	2.00	62.88
very high	17.25	2.00	1.82	4.04	122.80

Hexanoic lignin esters with ascending DS were synthesized successfully according to Table 12. The DS values for the medium and high samples are noticeable less than the ones of butyric lignin esters. Additional purification by precipitation explains this loss. The hexanoic ester with very high DS has a calculated DS value significantly higher than 100%. Most probably, not all impurities could be removed by the precipitation process. In addition, the big integral range could lead to an overestimation of the results.

3.5 Lignin nanoparticles

Lignin esters with different ester groups and DS (described above) were further used to prepare NPs. The influence of the varying hydrophobic groups and different DS on nanoparticle properties was subsequently analyzed.

3.5.1 Nanoparticle preparation

LNPs were synthesized via solvent exchange method with water as antisolvent according to Farooq et al. (Farooq et al. 2019).

acetone:water 3:1
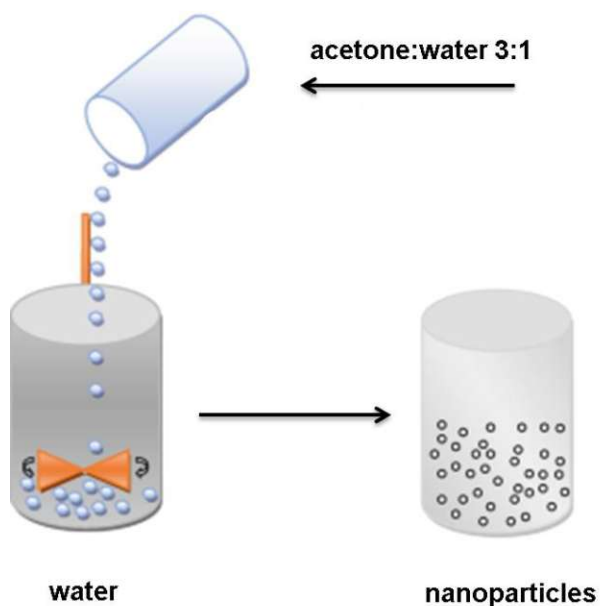
lignin esters derived from:

AA-M	IBA-M	HA-M	
AA-H	IBA-H	HA-H	native
AA-HH	IBA-HH	HA-HH	

prepared nanoparticles:

NP-AA-M	NP-IBA-M	NP-HA-M	
NP-AA-H	NP-IBA-H	NP-HA-H	NP-native
NP-AA-HH	NP-IBA-HH	NP-HA-HH	

water   nanoparticles

Scheme 3: Participation method for different lignin esters and their corresponding abbreviations. Native=blank, AA=acetic anhydride, IBA=isobutyric anhydride, HA=hexanoic anhydride, M=medium DS, H=high DS, HH=very high DS and NP=nanoparticle. The scheme was modified from (Kumar and Sharma, 2021).

As shown in Scheme 3, precipitation of the NPs occurred after dissolving the solid lignin esters in a mixture of acetone/water and subsequent dropwise addition of DI water under constant stirring. Overall, 10 NP samples were prepared starting with either Indulin AT (native) or modified lignin esters. Acetic, isobutyric and hexanoic lignin esters with a medium, high and very high DS respectively were used for NP synthesis. The 3 synthesized lignin esters from esterification of lignin via IBA (3.4.1) with varying DS (IBA-M, IBA-H, IBA-HH) and the 3 synthesized lignin esters from esterification of Lignin with HA (3.4.2) with varying DS (HA-M, HA-H, HA-HH) were taken for NP preparation as well as run 6 (high DS; AA-H) and run 8 (medium DS; AA-M) from acetylation of lignin via AA (3.2). Yet, the acetylated lignin with very high DS (AA-HH) could not be prepared with the here developed method. Therefore a large access of AA and 1 mmol Im were brought together at a temperature of 50 °C for 18 h (cf. isobutyric and hexanoic lignin esters with very high DS 3.4.1, 3.4.2) (Thielemans and Wool, 2004). After standard workup a DS of 112.28% was achieved. Evaluation was done identically to the other samples of *in situ* preparation of *N*-acetylimidazole method (3.2). But the aromatic and aliphatic signals in the corresponding ranges overlapped slightly resulting in a DS above 100%.

During NP preparation, the solvent for NP-HA-HH had to be adjusted to pure acetone in contrast to all other nanoparticle samples which were soluble in a mixture of

acetone/DI water. Most probably, the high amount of non-polar hydrocarbons of hexanoic ester caused this insolubility problem.

For these 10 NP samples a solid content 0.4 wt% was adjusted and a series of selected analysis (see below) were carried out in order to achieve detailed information of the structure, size and chemical behavior.

3.5.2 Particle diameter and zeta (ζ) potential analysis (Zetasizer)

Particle diameter and zeta (ζ) potential were analyzed for all 10 nanoparticle samples. The average of 3 measurements was taken for determination. Starting with size (diameter) analysis, measured using DLS technique, the corresponding values can be seen in Table 13.

Table 13: Average diameters (nm) and according standard deviations for all nanoparticle samples determined via Zetasizer.

Sample	Average diameter (nm)	SD
NP-native	94.59	0.50
NP-AA-M	71.50	0.36
NP-AA-H	59.69	0.59
NP-AA-HH	56.55	0.35
NP-IBA-M	73.11	0.39
NP-IBA-H	71.36	0.31
NP-IBA-HH	71.28	0.64
NP-HA-M	68.05	0.30
NP-HA-H	62.64	0.30
NP-HA-HH	78.13	0.48

In Table 13 the average diameters of 3 measurements respectively and their standard derivations (SD) are listed. The diameters are varying from 56.55 nm (NP-AA-HH) to 94.59 nm (NP-native). All IBA nanoparticles show similar diameters whereas NP-AA-M and NP-HA-HH possess significant deviations to the other respective lignin nanoparticle esters. Four of 10 NP samples underwent a size evaluation via AFM (see 3.5.3) as well. For graphical evaluation, bar charts were composed in Figure 15.
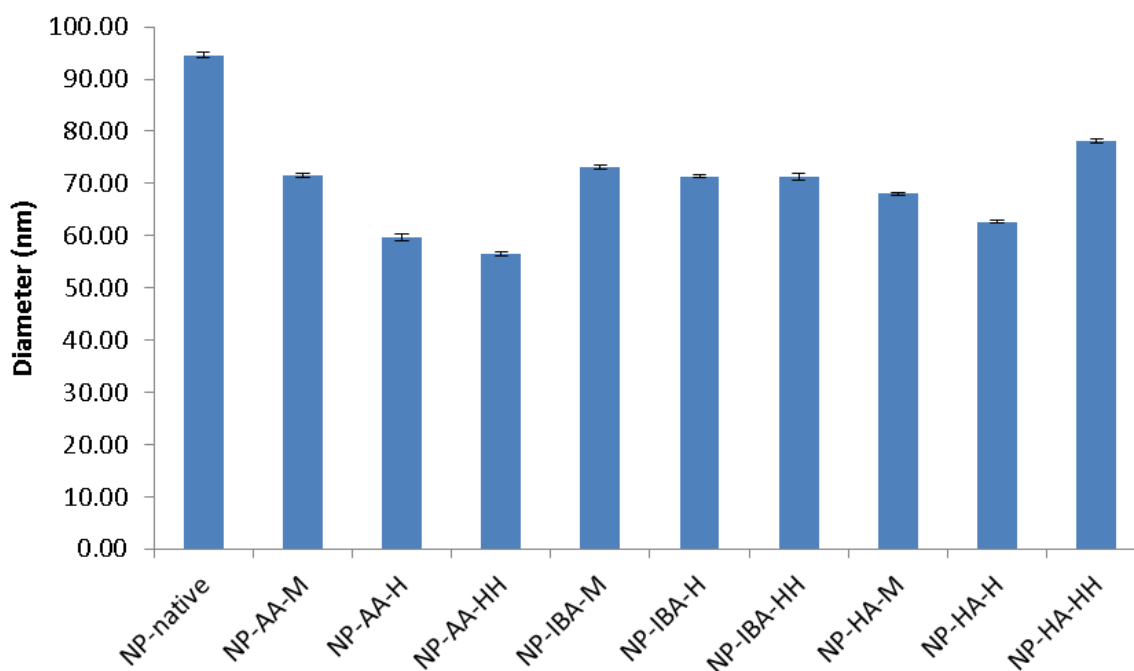
Figure 15: Average diameters (nm) and according error bars for all nanoparticle samples determined via Zetasizer.

In Figure 15 the particle diameters determined via Zetasizer show similar results for NP-AA-M, all NP-IBA and NP-HA-M. The size for other NPs varies widely.

Moreover, the ζ potential was determined for all NP samples and can be seen in Table 14.

Table 14: Average ζ potentials (mV) and according standard deviations for all nanoparticle samples determined via Zetasizer.

Sample	Average ζ potential (mV)	SD
NP-native	-21.0	0.9
NP-AA-M	-17.1	0.8
NP-AA-H	-23.2	1.6
NP-AA-HH	-30.7	1.3
NP-IBA-M	-22.8	1.3
NP-IBA-H	-22.1	1.2
NP-IBA-HH	-21.3	0.5
NP-HA-M	-20.4	0.2
NP-HA-H	-21.6	0.5
NP-HA-HH	-25.5	1.1

The ζ potential values in Table 14 give a minimum value of -30.7 mV and a maximum value of -17.1 mV. For acetylic and hexanoic lignin esters a descending tendency is recognized. The higher the DS the lower the ζ potential, as less of unmodified aromatic and aliphatic groups are available (Setälä et al., 2020). Isobutyric lignin esters show similar ζ potential values independent of the DS. The higher the value of ζ potential the lower the tendency of coagulation/self-assembly because the repulsive

forces exceed the attractive forces (Liu et al., 2019b). That can be a reason for the values of NP-native and all NP-IBA. The ζ potential values are graphically shown in Figure 16.
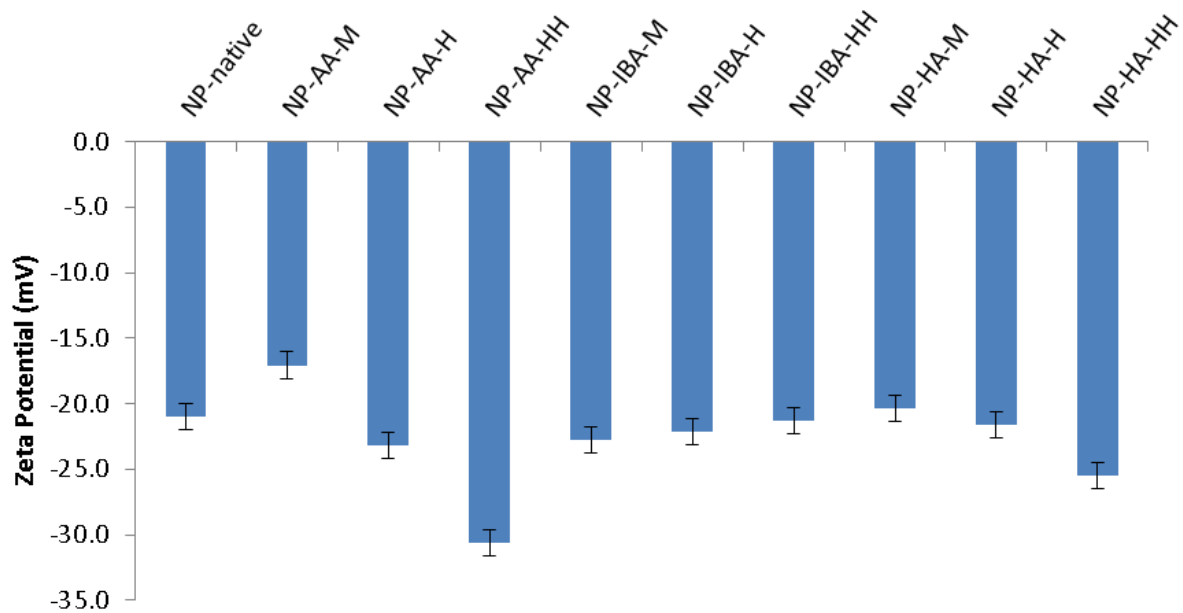
Figure 16: Average ζ potentials (mV) and according error bars for all nanoparticle samples determined via Zetasizer.

The trends and ζ potential values are shown in Figure 16. The descending trends of NP-AA and NP-HA indicate more stable nanoparticles because of increasing repulsive interactions, provoked by the higher presence of hydrophobic ester groups at the surface.

3.5.3 Atomic force microscopy (AFM)

AFM measurements were performed in order to achieve a detailed information about size, structure and the appearance of the nanoparticles at high zooms. The samples NP-native, NP-AA-HH, NP-IBA-H and NP-HA-H were investigated because they showed the smallest sizes with little standard deviation at Zetasizer measurement (cf. Table 13). 2 x 2 µm^2 images were prepared and evaluated on size. All images are provided with a color bar so as to distinguish the size in z-axis. The brighter the larger for each NP size (nm).
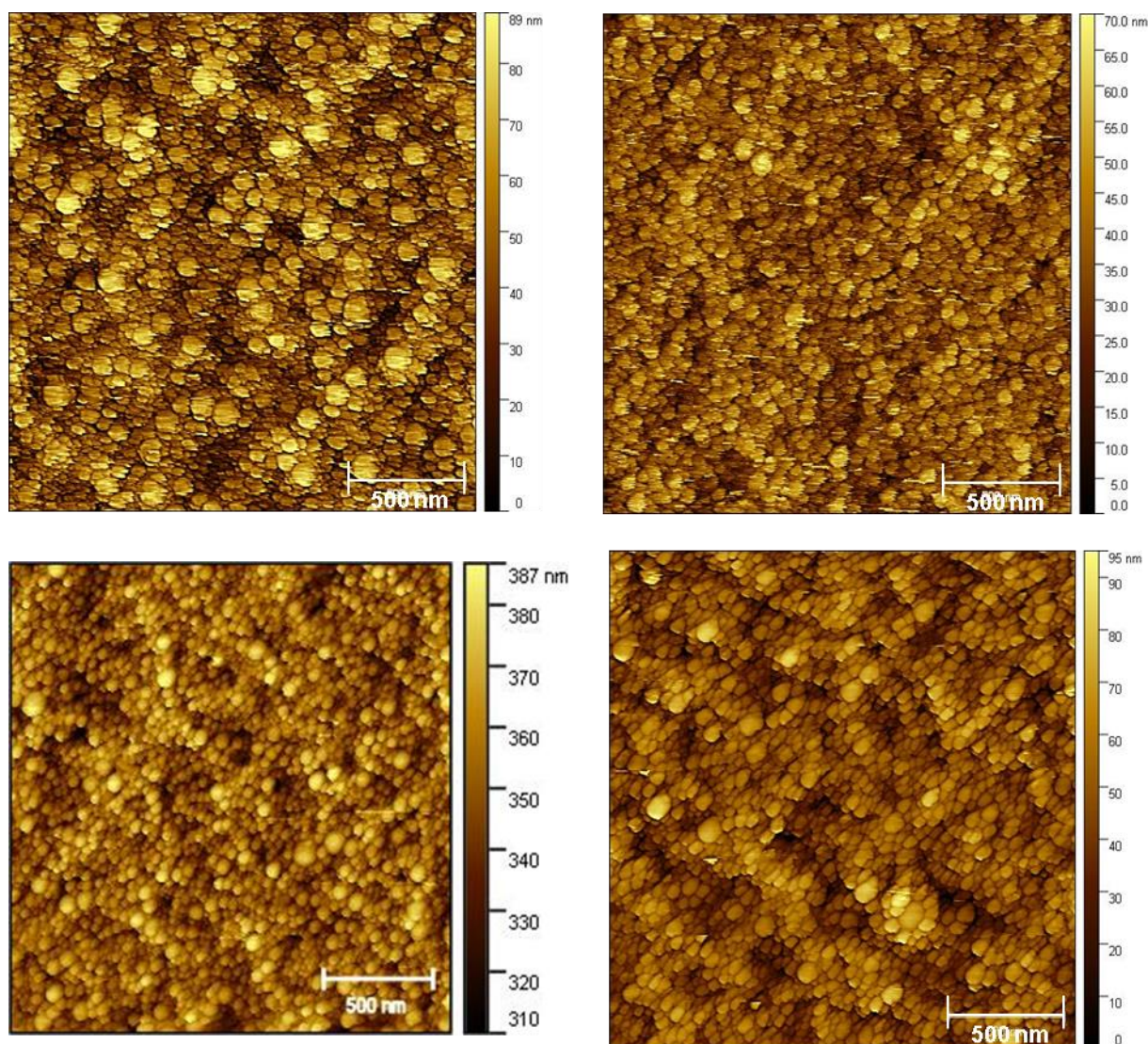
Figure 17: 2 x 2 µm^2 images for: NP-native (left top), NP-AA-HH (right top), NP-IBA-H (left bottom) and NP-HA-H (right bottom).

In Figure 17 the captured AFM images of the respective NP samples are illustrated. The NPs are densely packed with constant size distribution and spherical shape. The NPs were further investigated by size measurement with the determination program. The distance between two points were set and defined as diameter.

Table 15: Average diameters (nm) and according standard deviations for NP-native, NP-AA-H, NP-AA-HH and NP-IBA-H determined via AFM.

Sample	Average diameter (nm)	SD
NP-native	185.78	31.12
NP-AA-HH	121.97	23.26
NP-IBA-H	130.87	18.87
NP-HA-H	164.93	21.58

The average values of 25 size determinations (25 nanoparticles) and respective standard deviations are listed in Table 15 for each sample. Nanoparticles of acetylated lignin esters with very high DS (NP-AA-HH) possess the smallest, and the native nanoparticles (NP-native) show the largest diameters on average. The standard deviations are adequate taking the determination technique (distance measurement between two selected points) into account. For better comparability, a graphical evaluation based on Figure 16 was created too (see Figure 18)
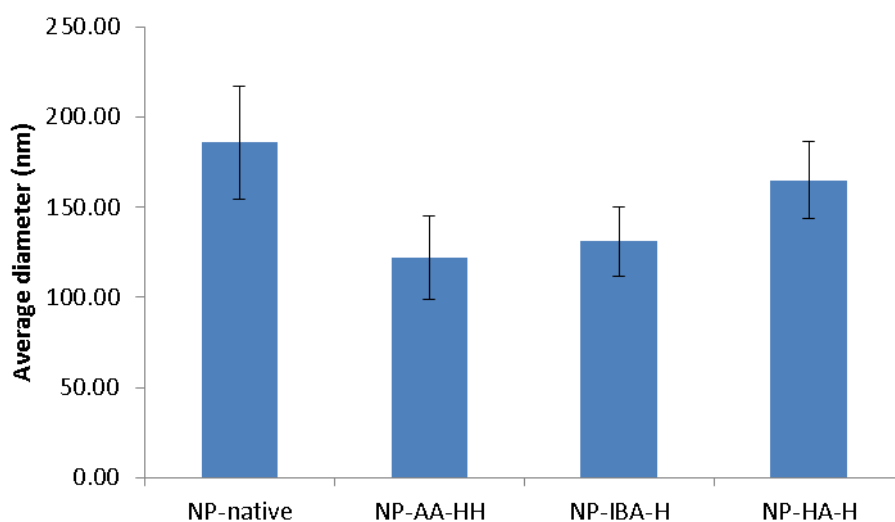
Figure 18: Average diameters (nm) and error bars for NP-native, NP-AA-H, NP-AA-HH and NP-IBA-H determined by AFM.

In Figure 18 native lignin shows the highest diameter on average, due to more hydrophilic interactions on the surface of unmodified lignin ester groups. The trend of increasing the average diameter depending on size of modified ester groups is noticed from NP-AA-HH to NP-HA-H (NP-IBA-H in between). This is not in accordance with the size evaluation, measured by Zetasizer (Figure 15) due to smaller NP sizes on average (Δ_{size} = 60-102 nm) for DLS measurements at 633 nm. Because UV-VIS measurements (3.5.5) showed overlapping absorbance values for this wavelength, the optical effects are expected to influence Zetasizer measurements. Therefore, the AFM determination is preferred for this thesis.

3.5.4 Fourier transformed infrared spectroscopy (FTIR)

Infrared spectra of all lignin NPs were performed intending to confirm complete reaction and on the other hand to obtain an overview and detect differences visually. Therefore NP-native was compared to AA-M in an attempt of allocating the bands (see Figure 19).
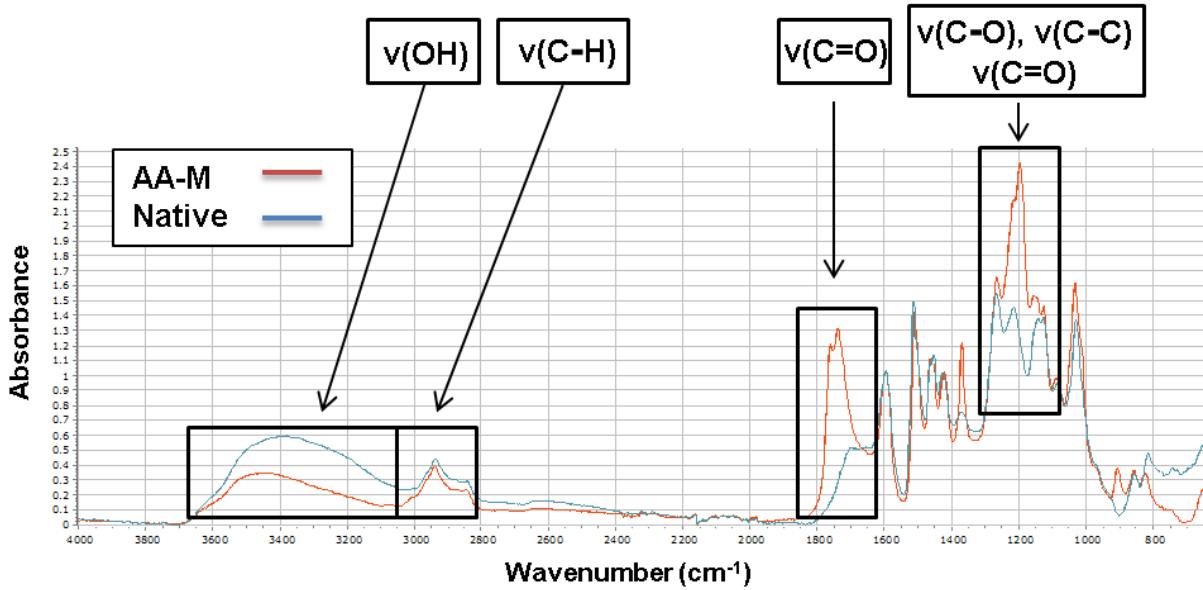
Figure 19: FTIR spectrum of the blank and acetic lignin ester nanoparticles with marked areas and corresponding chemical bonds.

As expected, the OH absorption band at 3100-3600 cm^{-1} reduced and the C=O at 1750 cm^{-1} stretch band increased drastically which is in accordance to an esterification reaction. Furthermore, the absorption band at 2800-3000 cm^{-1} can be allocated to C-H stretches and a cluster of bands at 1100-1300 cm^{-1} to C-C, C-O and C=O stretches (Fox and McDonald, 2010).

A spectrum with all nanoparticle samples was determined as well in order to demonstrate the difference between the modified and unmodified samples. The range was set from 850-1900 cm^{-1} and displayed in Figure 20.
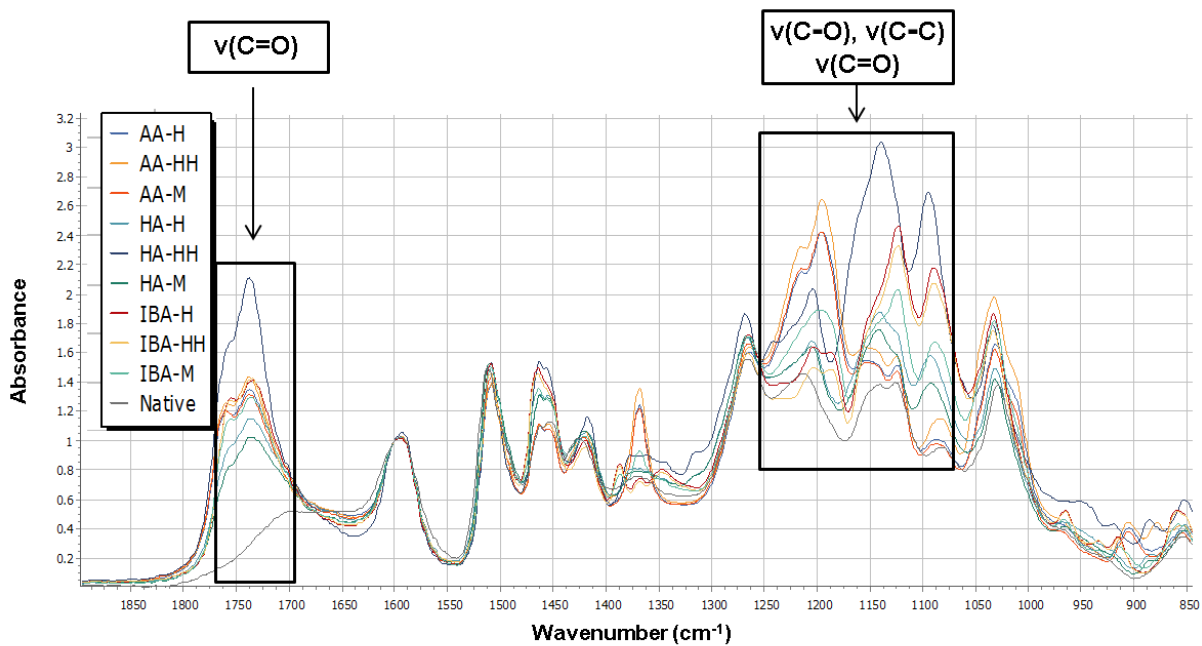
Figure 20: FTIR spectra of all nanoparticles in the range of 850-1900 cm⁻¹ with marked areas and corresponding chemical bonds.

The lowest curve (grey) belongs to NP-native in the marked areas in Figure 20. A conversion to lignin esters is detected by comparing the unmodified samples to the others. The C=O stretch at 1750 cm⁻¹ is very high for NP-HA-HH indicating the highest DS value. Obviously, for NP-native no band for C=O stretch was allocated. C-C, C-O and C=O stretches at 1100-1300 cm⁻¹ present a very diffuse picture with NP-HA-HH as highest value too.

3.5.5 Ultraviolet – visible spectroscopy (UV-VIS)

UV-VIS spectra from 200-800 nm of all nanoparticle samples were recorded and collected in Figure 21 in order to gain absorbance information at UV-VIS.
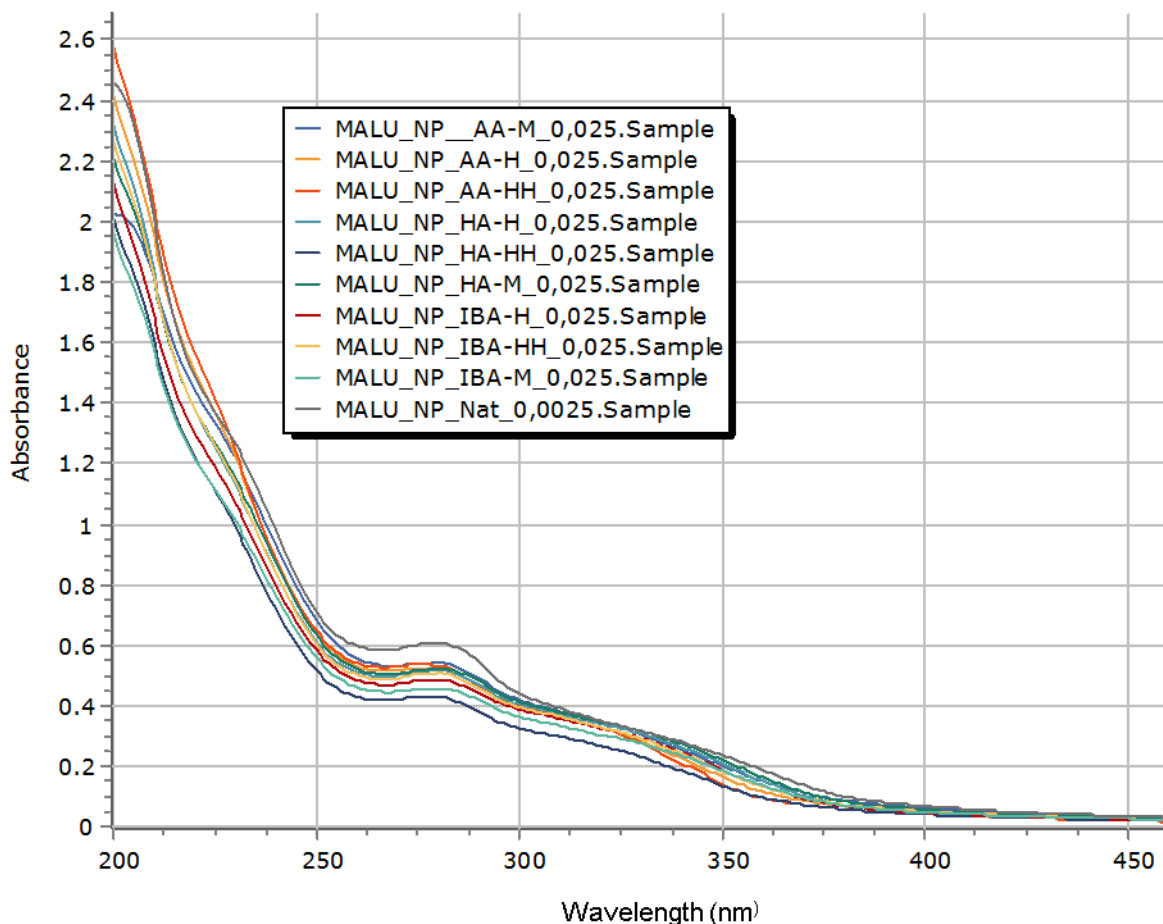
Figure 21: UV-VIS spectra of all nanoparticle samples.

The UV-VIS spectra were actually measured between 200-800 nm but for analysis a closer look was taken at the range between 200-450 nm due to a plateau in the area of 450-800 nm. A maximum at 280 nm can be detected which would be "considered as primary wavelength for quantification of lignin" (Lee et al., 2013; Zhang et al., 2017). Absorbance values ≤0.1 are in the visible wavelength region from 400-800 nm and explain the hardly visible nanoparticles for the adjusted concentration.

3.5.6 Contact angle (θ) measurement

Contact angle (θ) measurements were carried out in order to achieve information of surface properties of nanoparticle samples. During AFM and microscopy analysis (see 3.5.8, 3.5.3) shapes of elongated partly rising threads were identified on which the drops of water were placed. The samples were prepared by drying in the fume hood overnight. They were measured 3 times on different locations of the micro slides. Measurement times were adjusted to 20 s each and evaluation was done by comparing the curve progression (Figure 22) as well as the θ (Figure 23) after 1 s and 15 s respectively.
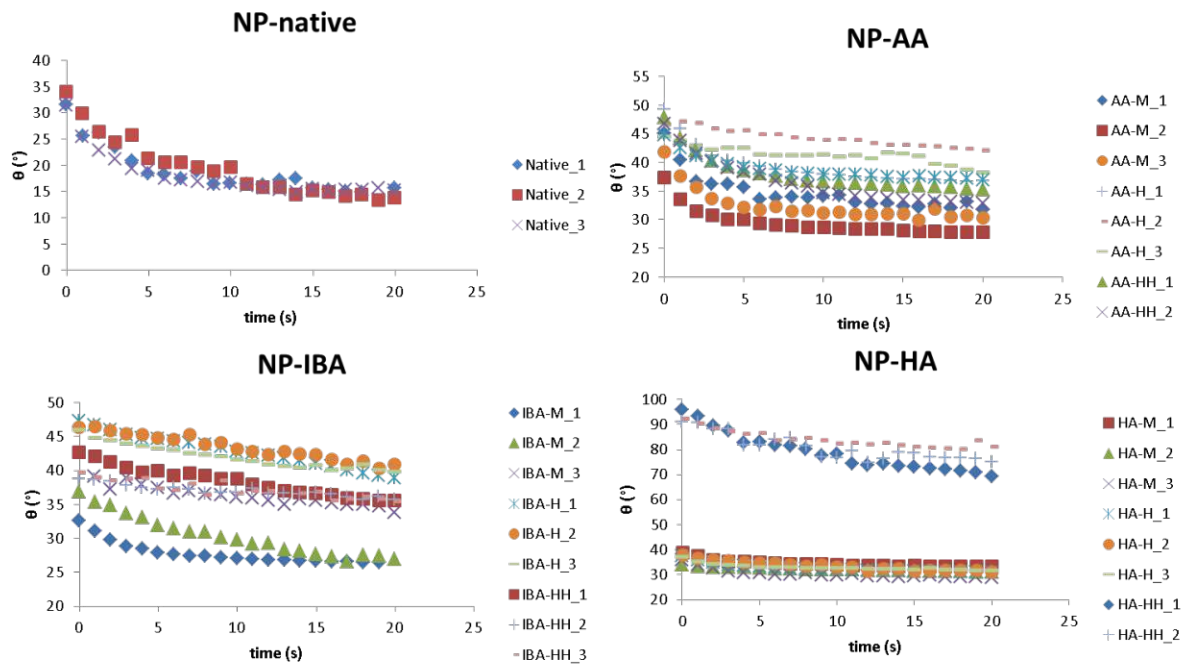
Figure 22: Curve progressions of θ (°) against time (s) for all nanoparticle samples during 20 seconds in total.

In Figure 22 the development of changing θ for 20 s is illustrated whereby the graphs were separated according to their type of modification. Over time, all nanoparticle samples show a decrease of θ due to surface absorption until they reached a plateau. NP-HA-HH clearly possesses the highest θ on average at any time measured. The long non polar chains and a very high DS support this hydrophobic behavior with θ up to 100°. To get a more comprehensive overview, the distinct θ values at t = 1 s and t =15 s are summarized in Figure 23.
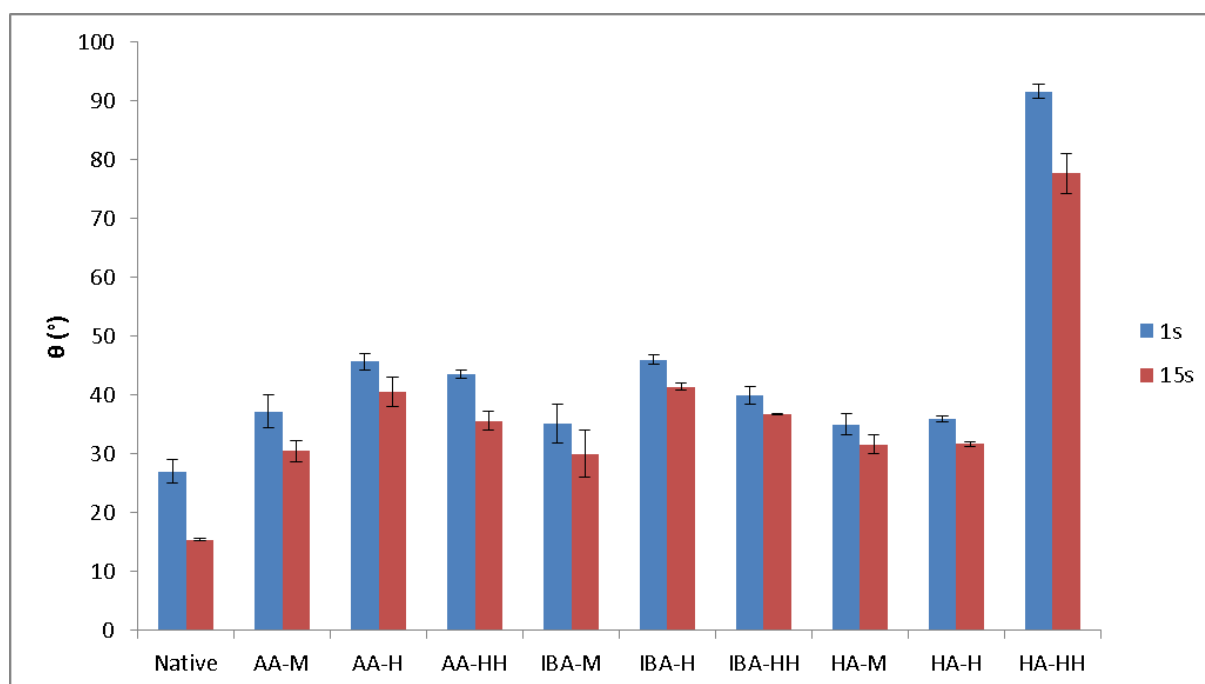
Figure 23: Average θ values (°) after 1 s and 15 s with error bars for all nanoparticles.

Apparently, the θ decreases over time (Figure 23). It can be seen that the unmodified nanoparticles have the lowest values with about 28° and 15° respectively because of missing ester groups and thus smaller contact area. All nanoparticle samples with medium (lowest) DS show the lowest θ. Acetic and isobutyric lignin nanoparticle esters with high DS display higher θ than those with very high DS. The type of ester does not influence the θ significantly even though NP-HA-HA possesses θ values. This nanoparticle sample was dissolved in pure acetone (all other NPs with acetone/water 3:1) for NP preparation and more hydrophobic ester groups on the surface developed consequently. In the literature, surfactant nanoparticles with increasing hydrophobicity were prepared by esterifying Indulin AT with different anhydrides (An et al., 2019), whereas all samples possessed relatively small θ compared to the native sample.

3.5.7 Pendant Drop measurement

The interfacial interactions of the nanoparticles were studied by pendant drop analysis (nanoparticle in water/air interface). The respective nanoparticle in water dispersion was pushed through a steel needle to obtain a stable droplet. The shape of this droplet was captured overtime to measure the time-dependent interfacial tension (up to 800 s). In addition, two defined time points were selected, t = 400 s and t = 600 s, to compare the values.
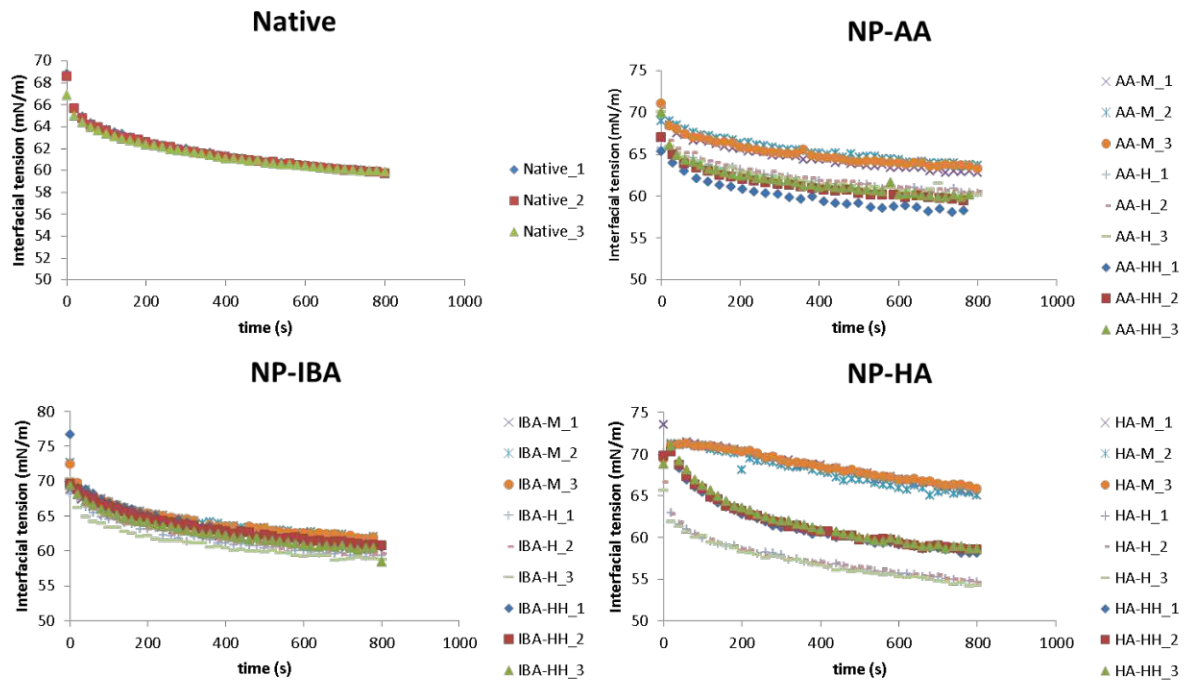
Figure 24: Curve progressions of interfacial tension (mN m⁻¹) against time (s) for all nanoparticle samples during 20 seconds in total

The progressions show a steady state after a few seconds that leads to a plateau with time (Figure 24). The interfacial tension decreases for all NP samples over time possibly due to absorption of air. As soon as a saturated coverage is built a steady state is reached (Zhang et al., 2017). Minimal DS effects on the interfacial tension are visible for NP-IBA samples alike NP-AA samples. Hexanoic lignin esters show the biggest difference and the differences between the individual samples is further shown in Figure 25 comparing the individual interfacial tension values at 400 and 600 s.
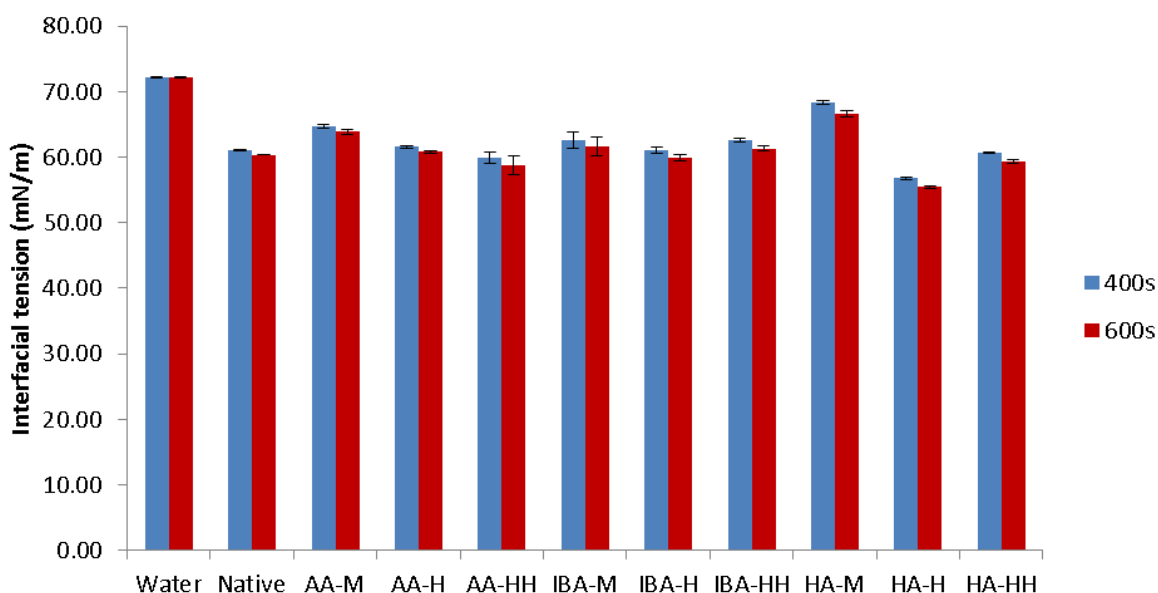
Figure 25: Average interfacial tension values (mN m^{-1}) after 1 s and 15 s with error bars for all nanoparticles.

In case of acetylated lignin NPs the interfacial tension decreases with increasing DS. Isobutyric lignin ester nanoparticles behave very similar independent from the DS. On the other hand, a significant decrease of interfacial tension is determined from NP-HA-M to NP-HA-H; however, the trend does not continue with interfacial tension values of NP-HA-HH in between. All modified lignin NP samples possess smaller interfacial tension than the reference water, and are hence surface active. But the unmodified (NP-native) sample has comparable or smaller surface tension than all modified samples (except NP-HA-H for which a 5 mN m^{-1} lower surface tension is determined). Therefore, a NP structure with mostly hydrophobic functional groups (ester) in the core and hydrophilic functional groups (hydroxyl, carboxyl) at the surface is suggested. This structure was studied for example by Sipponen et al. (Sipponen et al., 2020) for lauric and oleic kraft lignin esters, as well as Zou et al. (Zou et al., 2021) for .kraft lignin-epoxy hybrid nanoparticles. It is assumed that through NP preparation (dropping dissolved lignin esters in aqueous acetone on water) this particular structure occurs. The solvent (acetone) and anti-solvent (water) composition therefore favor the distribution of functional groups through self-assembly during participation process of the NPs.

3.5.8 Preparation of films and microscopy

The self-assembly of the nanoparticles during film formation on glass plates was studied by optical microscopy. It was decided to investigate half of the 10 nanoparticle samples (NP-native, NP-HA-H, NP-AA-M, NP-AA-H and NP-AA-HH)

because the NP-AA samples with varying DS showed the most significant differences in pendant drop measurements (interfacial tension), size and ζ potential measurements (Zetasizer).

The samples were prepared by dropping the respective nanoparticle dispersion onto a micro slide via pipette and subsequent drying in the fume hood overnight. Images of 3 times zoom (in order to achieve a good overview) and 20 times zoom (for detailed information) were taken and illustrated in Figure 26 - Figure 28.
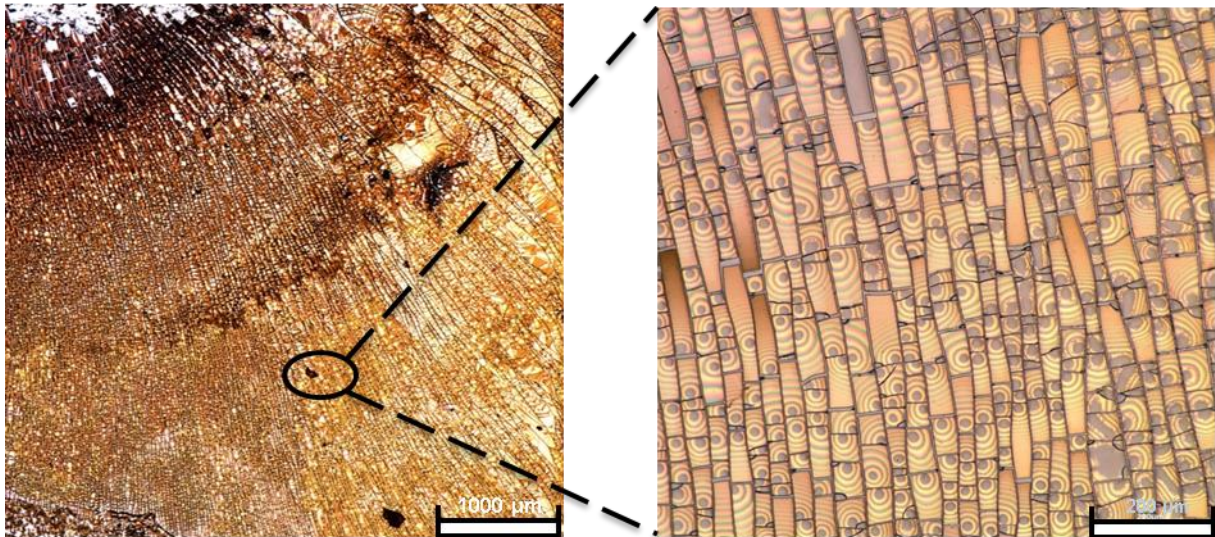
Figure 26: Images of native nanoparticles (NP-native) with 3 times zoom and 20 times zoom from left to right.

The left image with 3x zoom in Figure 26 shows the drying manner of lignin nanoparticle samples. The higher the lignin concentration in a specific area the darker and decreasing in waves from top left to bottom right. The samples on the slides did not generate a smooth film but a rough surface with cracks and elongated partly rising areas especially visible at the edges. The individual regions can be seen in the right image with 20x zoom. An ordered and square structure of the parts itself are detected. Starting at a certain nanoparticle (circular dark point) a wavy decrease of concentration (from dark to bright) is observed. Apparently, this pattern is favored energetically.
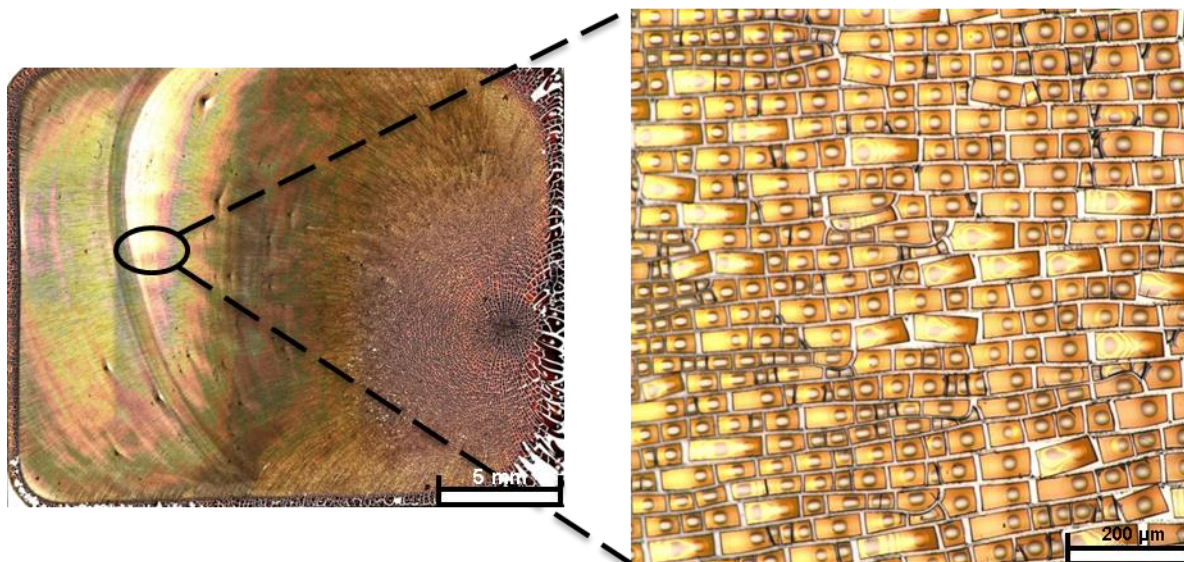
Figure 27: Images of hexanoic lignin ester nanoparticles (NP-HA-H) with 3 times zoom and 20 times zoom from left to right.

Similar analysis to Figure 27 can be determined as to the NP-native sample Figure 26). In the left picture with lower zoom one does even see the concentration progression in color as well as the cracks and rising areas (especially at the edges) more clearly. At the edges the coffee ring effect occurs (Wong et al., 2011). Furthermore, light scattering in the visible area is noticed in an area with little nanoparticle concentration. In that particular region an image with higher zoom was recorded (right side, Figure 27). More clear cracks and bigger nanoparticles (dots) which protrude as well as an even more ordered and square structure (like bricks) is visible in comparison to the native nanoparticle film. Interestingly, only in some little bricks the coffee ring effect occurs concentrating the lignin nanoparticles to the rim. A centered lignin dot with high concentration at the outside is favored. This circumstance maybe simply occurred during film preparation. A planar oriented micro slide produces NP arrangements as in Figure 27 during evaporation of solvent and micro slides with tilt orientation (not planar) lead to arrangements as Figure 26.
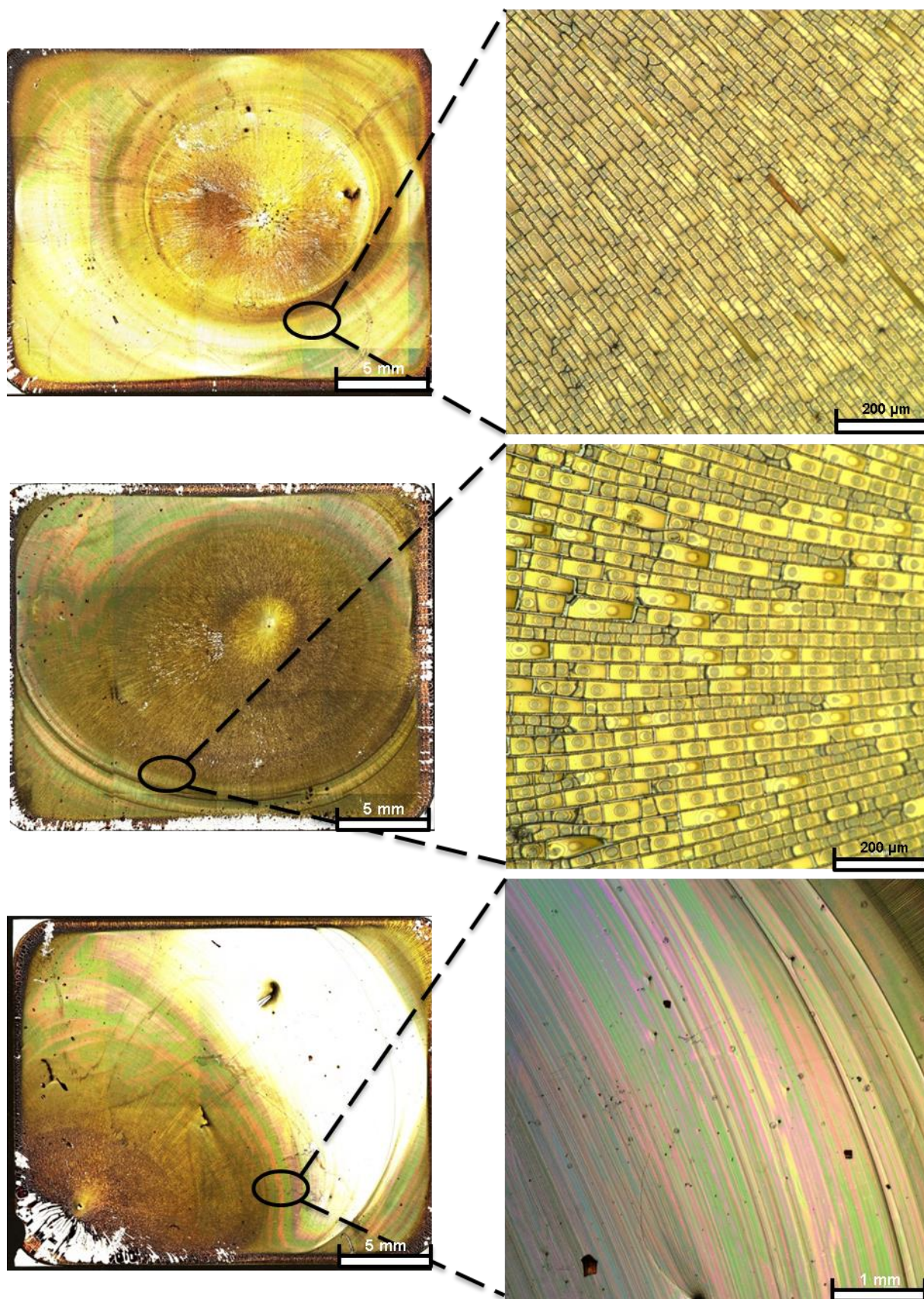
Figure 28: Images of acetylated lignin nanoparticles with 3 times zoom and 20 times zoom from left to right. With acetylated lignin nanoparticles with medium DS (NP-AA-M) at the top, acetylated lignin nanoparticles with high DS (NP-AA-H) in the middle and acetylated lignin nanoparticles with very high DS (NP-AA-HH) at the bottom.

Microscopic images of all acetylated lignin nanoparticles were performed and illustrated in Figure 28. A distinctive coffee ring effect of NP-AA-M is detected resulting in a dark rim (high concentration of NPs) and bright remaining surface. The images of NP-AA-M (top) and NP-AA-H (middle) are comparable to NP-HA-H (Figure 27) with ordered structures and nanoparticles centered in the middle. The NP-AA-HH sample (bottom) has a circular area of high concentration at the left bottom of the sample and therefore just little concentration at the remaining surface. Hence light scattering occurred at the transition which was captured in the bottom right picture. Green, purple and slightly blue circle lines are visible due to thin film interference (Cong and Cao, 2004).

4 Experimental part

4.1 Materials

4.1.1 Chemicals and starting materials

All chemicals were used as received (cf. Table 16) if not otherwise described.

Table 16: List of chemicals

Name	Specification	Supplier
Indulin AT	softwood kraft lignin	MeadWestvaco Corp
N-Acetylimidazole	≥98%	TCI
Acetic Anhydride	≥99%	Sigma Aldrich
Hexanoic Anhydride	≥97%	Sigma Aldrich
Isobutyric Anhydride	≥95%	TCI
Imidazole	≥99%	Sigma Aldrich
Acetone	≥99.5%	Sigma Aldrich
sodium chloride	≥99.0	Sigma Aldrich

4.2 Methods: esterification of lignin

4.2.1 Pre-treatment of starting materials

4.2.1.1 Dry lignin

Dry Indulin AT was prepared by vacuum drying at 40 °C for at least 72 h.

4.2.1.2 Lignin with different moisture contents

The moisture content of Indulin AT was adjusted by adding certain amount of water via a pipette and subsequent mixing with a spatula for 5 min. Five batches were prepared in total (see Table 17) and reproduced according to the procedure when necessary.

Table 17: Amount of water needed for adjusting certain moisture content and associated masses for Indulin AT.

Indulin AT (mg)	Dry indulin AT (mg)	Moisture content (wt%)	Water (µl)
5000	4775	9.9	247.725
8000	7640	17.3	961.72
3000	2865	24.6	569.79
1500	1432.5	30	362.25

4.2.1.3 Imidazole (Im)

Before its usage for synthesis Im was grinded in a kitchen coffee grinder in order to achieve a fine powder.

4.2.2   Acetylation of lignin via *N*-acetylimidazole

N-acetylimidazole and 500 mg Indulin AT were ball-milled (Retsch CryoMill, Retsch GmbH, Germany) for 30 min under solvent-free conditions according to Scheme 1 (ball mill). Four stainless steel balls (8 g, 0.5 mm diameter) were used for homogeneous mixing at 25 Hz without cooling. The reaction is induced as soon as both substances were brought into contact and stopped by quenching with 40 mL DI water followed by shaking for 24-72 h. The sticky dark red/brownish mixture was transferred into a 50 mL centrifugation vial and 10 Vol% of 1 M AcOH was added. The dispersion was vortexed, centrifuged for 30 min at 5000 rpm and subsequently decanted. This procedure was repeated twice. Afterwards the mixture was further washed with 40 mL DI water and got vortexed, centrifuged (30 min at 5000 rpm) as well. After freeze-drying under vacuum at 40 °C, acetylated lignin was obtained as a light red, brownish solid.

The relation of the factors: reaction time, moisture content and equivalents of *N*-acetylimidazole were investigated with the DoE software "Design – Expert 13". Therefore, a quadratic model with spherical central composite design, two replicates of factorial points and four center points was compiled (Table 18, Table 19).

Table 18: Factors from acetylation of lignin via *N*-acetylimidazole

Factor	Name	Units	Minimum	Maximum
A	Moisture content	%	4.50	30.00
B	*N*-acetylimidazole	Eq	0.34	1.15
C	Reaction time	h	0.50	3.00

The ranges of the three factors were set as illustrated in Table 18. Moisture content at standard conditions was known to be 4.5% and higher contents were prepared as described in 4.2.1.2. Longer reaction time than 0.5 h was put into practice by 30 min ball-milling followed by respective dwelling time.

Table 19: Values of the factors to be analyzed for acetylation of lignin via *N*-acetylimidazole

Run	Moisture content (%)	Reaction time (h)	*N*-acetylimidazole (eq)	*N*-acetylimidazole (mmol)	*N*-acetylimidazole (mg)
1	24.60	2.47	0.55	1.28	196.64
2	17.30	1.75	0.74	1.74	267.39
3	9.90	1.03	0.48	1.13	173.44
4	9.90	1.03	0.91	2.14	327.61
5	17.25	1.75	0.74	1.74	267.39
6	17.25	1.75	1.15	2.68	411.37
7	17.25	3.00	0.74	1.74	267.39
8	17.25	1.75	0.34	0.80	123.41

9	24.60	1.03	0.55	1.28	196.64
10	17.25	1.75	0.74	1.74	267.39
11	9.90	2.47	0.91	2.14	327.61
12	30.00	1.75	0.83	1.93	296.34
13	24.60	2.47	1.03	2.42	371.43
14	9.90	2.47	0.48	1.13	173.44
15	17.25	1.75	0.74	1.74	267.39
16	17.25	0.50	0.74	1.74	267.39
17	4.50	1.75	0.64	1.49	227.96
18	24.60	1.03	1.03	2.42	371.43
19	17.25	1.75	0.74	1.74	267.39
20	4.50	1.75	0.64	1.49	227.96
21	30.00	1.75	0.83	1.93	296.34
22	17.25	1.75	0.74	1.74	267.39
23	17.25	0.50	0.74	1.74	267.39
24	17.25	1.75	1.15	2.68	411.37
25	17.25	3.00	0.74	1.74	267.39
26	17.25	1.75	0.34	0.80	123.41

In Table 19 the varying parameters, including moisture content, *N*-acetylimidazole and reaction time are shown as well as the corresponding mmol and mg of *N*-acetylimidazole. The Software "Design – Expert 13" automatically creates a table in random order.

In order to validate the experiment, two more runs were carried out under the same procedure (Table 20).

Table 20: Values of the validation experiments for acetylation of lignin via *N*-acetylimidazole

Run	Moisture content (%)	Reaction time (h)	*N*-acetylimidazole (eq)	*N*-acetylimidazole (mmol)	*N*-acetylimidazole (mg)
27	17.25	1.87	1.15	2.68	411.37
28	17.25	1.87	1.15	2.68	411.37

The validation values of moisture content, reaction time and equivalents of *N*-acetylimidazole in Table 20 are close to those of the center points but were predicted by the DoE software.

Collectively, all investigated data and associated mass yields are shown in Table 21

Table 21: Moisture content (%), reaction time (h), amount of *N*-acetylimidazole (eq) and achieved mass yields in (mg, %) for all syntheses.

Run	Moisture content (%)	Reaction time (h)	*N*-acetylimidazole (eq.)	Mass yield (mg)	Mass yield (%)
1	24.60	2.47	0.55	548	102.98
2	17.30	1.75	0.74	458	84.24
3	9.90	1.03	0.48	473	89.52
4	9.90	1.03	0.91	504	91.05

5	17.25	1.75	0.74	485	89.20
6	17.25	1.75	1.15	451	79.51
7	17.25	3.00	0.74	474	87.18
8	17.25	1.75	0.34	479	92.08
9	24.60	1.03	0.55	506	95.09
10	17.25	1.75	0.74	481	88.47
11	9.90	2.47	0.91	464	83.82
12	30.00	1.75	0.83	508	92.63
13	24.60	2.47	1.03	433	77.22
14	9.90	2.47	0.48	455	86.12
15	17.25	1.75	0.74	472	86.81
16	17.25	0.50	0.74	464	85.34
17	4.50	1.75	0.64	455	84.69
18	24.60	1.03	1.03	521	92.92
19	17.25	1.75	0.74	433	79.64
20	4.50	1.75	0.64	432	80.41
21	30.00	1.75	0.83	510	92.99
22	17.25	1.75	0.74	489	89.94
23	17.25	0.50	0.74	481	88.47
24	17.25	1.75	1.15	465	81.97
25	17.25	3.00	0.74	454	83.50
26	17.25	1.75	0.34	483	92.85
27	17.25	1.87	1.15	519	91.49
28	17.25	1.87	1.15	546	96.25

4.2.3 Acetylation of lignin via *in situ* preparation of *N*-acetylimidazole

500 mg Indulin AT with a moisture content of 17.25% were put into a 50 mL centrifugation vial. AA and Im were added consecutively, resulting in an *in-situ* preparation of *N*-acetylimidazole under solvent-free conditions (see Scheme 1). The mixture was stirred with a spatula for 5 min, obtaining a viscous, dark red substance. The reaction was stopped by quenching with 40 mL DI water after 2 h followed by shaking for 24 h. For workup, 10 Vol% of 1 M AcOH was added then vortexed and centrifuged for 30 min at 5000 rpm followed by decantation. Purification was done by washing with 40 mL DI water and centrifugation (30 min at 5000 rpm). The workup- as well as the purification procedure was repeated twice. After drying at 80 °C for 72 h acetylated lignin was achieved as a light brownish solid.

Comparable to 4.2.2 the acetylation of lignin with *in-situ* prepared *N*-acetylimidazole under solvent-free conditions was carried out with "Design – Expert 13". It comprises a quadratic model with spherical central composite design four central points and no replicates. The factors for investigation are: equivalents of AA and the ratio of AA

(eq) to Im (eq) whereby reaction time and moisture content remain constant (Table 22, Table 23).

Table 22: Factors from acetylation of lignin with AA

Factor	Name	Units	Minimum	Maximum
A	AA	eq	0.78	1.56
B	AA : Im	eq	1.00	3.00

The selected minimum and respective maximum values can be seen in Table 22.

Table 23: Values of the factors to be analyzed for acetylation of lignin with AA.

run	AA (eq)	AA (mmol)	AA (mg)	AA (eq) / Im (eq)	Im (mmol)	Im (mg)
1	1.17	3.82	0.36	2.00	1.91	130.10
2	1.45	4.72	0.45	2.71	1.74	118.77
3	1.17	3.82	0.36	1.00	3.82	260.19
4	1.17	3.82	0.36	2.00	1.91	130.10
5	1.17	3.82	0.36	2.00	1.91	130.10
6	1.56	5.10	0.48	2.00	2.55	173.46
7	1.17	3.82	0.36	2.00	1.91	130.10
8	0.90	2.92	0.28	2.71	1.08	73.46
9	1.45	4.72	0.45	1.29	3.65	248.68
10	0.78	2.55	0.24	2.00	1.27	86.73
11	0.90	2.92	0.28	1.29	2.26	153.81
12	1.17	3.82	0.36	3.00	1.27	86.73

The calculated data of the DoE and their associated values in mmol and mg are listed in Table 23. The implementation is supposed to be done in a random order, prescribed by Design – Expert 13.

Collectively, all investigated data and associated mass yields are shown in

Table 24: AA (eq), ratio of AA (eq) to Im (eq) and achieved mass yields in (mg, %) for all syntheses

Run	AA (eq)	AA (eq) / Im (eq)	Mass yield (mg)	Mass yield (%)
1	1.17	2.00	520	91.42
2	1.45	2.71	492	84.10
3	1.17	1.00	483	84.92
4	1.17	2.00	423	74.37
5	1.17	2.00	314	55.20
6	1.56	2.00	495	83.65
7	1.17	2.00	470	82.63
8	0.90	2.71	438	79.26
9	1.45	1.29	459	78.46
10	0.78	2.00	448	82.07
11	0.90	1.29	462	83.61

| 12 | 1.17 | 3.00 | 483 | 84.92 |

4.2.4 Esterification of lignin via isobutyric anhydride (IBA)

In Scheme 2 (R=isobutyl) the synthesis pathway is shown. The esterification synthesis with IBA was performed twice in order to achieve two different samples distinguishable by their DS. The mole of IBA and Im – requisite for this solvent-free *in-situ* synthesis- were adapted from Table 3 (run 6, run 11), thus receiving medium and high DS.

For this purpose 500 mg Indulin AT (17.25% moisture content) were first put into a centrifugation vial. IBA (2.92 mmol, 0.90 eq; 5.10 mmol, 1.56 eq) was added dropwise via syringe and Im (2.26 mmol, IBA/Im 1.29 eq; 2.55 mmol, IBA/Im 2 eq) was added right after. The dark brownish/red, viscous mixtures were stirred with a spatula for 5 min and were quenched after 2 h with 40 mL DI water followed by shaking for 24 h each. The crude products were centrifuged (20 min at 5000 rpm) and decanted. 40 mL EtOH/H_2O, (1:1, v/v) were added then vortexed centrifuged and decanted. This procedure was performed twice for workup. Double washing with 40 mL DI water and identical intermediate steps as workup were carried out for purification. After 48 h drying at 80 °C the light brown, powdery solids were obtained (medium: 459 mg, 83%, high: 508 mg. 86%).

4.2.5 Esterification of Lignin via hexanoic anhydride (HA)

Similar to 4.2.4 (Esterification of lignin via isobutyric anhydride) the synthesis (see Scheme 2) was performed twice desirably achieving similar DSs (medium and high). Consequently, same mole and equivalents of HA (2.92 mmol, 0.90 eq; 5.10 mmol, 1.56 eq) and Im (2.26 mmol, HA/Im 1.29 eq; 2.55 mmol, HA/Im 2 eq) were added to 500 mg 17.25 mg Indulin AT. Further synthesis, workup and purification were done identical, achieving hexanoic esterified lignins as brownish dark red hunks. Due to inhomogeneous mixing during workup and purification, both samples underwent additional purification treatments. 4 mL acetone were added and the suspensions got shaken for 4 h. The completely dissolved crude products were transferred in pasteur pipettes and dropped on 70 mL hexane. Double washing with 40 mL hexane followed by vortexing, centrifugation (5000 rpm, 20 min), decantation and drying at 80 °C for 24 h resulted in red powdery solids respectively (medium: 344 mg, 62%, high: 394 mg, 67%).

4.2.6 Esterification of Lignin with very high degree of substitution

For esterification of lignin with different anhydrides (AA, IBA and HA), achieving very high DSs similar synthesis pathways to Thielemans and Wool (Thielemans and Wool, 2005) were performed with Im as catalyst. An excess of respective anhydride, catalytic amounts of Im (1 mmol) and no solvents were used for syntheses.

4.2.6.1 Acetic anhydride

AA (11.43 mmol, 3.50 eq) was put into a round bottom flask with a magnetic stir bar. 500 mg dry Indulin AT and Im (1 mmol, 11.44 eq) were added while stirring vigorously. The temperature was set to 50 °C and the synthesis was carried out for 18 h. The light brown viscous suspension was quenched with 50 mL EtOH/H_2O, (1:1, v/v) and was further stirred for 2 h at RT. The crude product was washed with 40 mL EtOH/H_2O and subsequent 40 mL DI water. Each purification step was performed twice while vortexing, centrifugation (5000 rpm, 20 min), decantation was done in between. After drying at 80 °C for 24 h acetylated lignin with very high DS was obtained as light brown solid (471 mg, 67%).

4.2.6.2 Isobutyric anhydride (IBA)

IBA (5.95 mmol, 1.82 eq), 500 mg dry Indulin AT and Im (1 mmol, 5.95 eq) were mixed vigorously in a round bottom flask with stirring bar at 50 °C. After 24 h the suspension was quenched with 50 mL EtOH/H_2O, (1:1, v/v). Additional stirring for 3 h at RT led to the crude product, which was washed twice with 40 mL EtOH/H_2O, (1:1, v/v) using a centrifuge (5000 rpm, 15 min). After purification via double washing with DI water, centrifugation (5000 rpm, 15 min) and subsequent drying at 80 °C for 72 h isobutyric lignin ester was obtained as light brown solid (384 mg, 63%).

4.2.6.3 Hexanoic anhydride (HA)

HA (4.04 mmol, 1.24 eq) was put into a round bottom flask with stirring bar. 500 mg dry Indulin AT and Im (1 mmol, 4.04 eq) was added while stirring rigorously and the temperature was increased to 50 °C. The very viscous dark red suspension was stirred for 24 h, quenched with 50 mL EtOH/H_2O, (1:1, v/v) and further stirred for 3 h at RT. The mixture got stuck at the glass wall partially and was transferred in a centrifugation vial with a spatula. The crude product was washed with 40 mL EtOH/H_2O, (1:1, v/v) and centrifuged (5000 rpm, 15 min) twice each. 40 mL DI water was added twice for purification followed by centrifugation at 5000 rpm for 15 min respectively. After drying at 80 °C for 72 h a big dark red hunk was obtained because

of inhomogeneity. Hence 4 mL acetone were added and the suspension got shaken until complete dissolution (3 h). The mixture was transferred into a pasteur pipette portion wise and added to 70 mL hexane drop by drop. After double washing with 40 mL hexane followed by vortexing, centrifugation (5000 rpm, 20 min), decantation and drying at 80 °C for 24 h hexanoic lignin ester was obtained as dark red powdery solids (382 mg, 67%)

4.2.7 Lignin nanoparticles

Synthesis of lignin nanoparticles were carried out using the solvent exchange method (Österberg et al., 2020). Nine esterified lignin samples and the blank sample were used for preparation following the procedure of Farooq et al. (Farooq et al., 2019) (see Scheme 3). The 9 lignin samples can be split into 3 acetic, isobutyric and hexanoic esters respectively each with a DS of medium, high and very high. For isobutyric and hexanoic lignin esters the 3 respective samples synthesized (4.2.4, 4.2.5) were used for NP preparation apparently. Run 6 and run 8 of acetylation of lignin with AA (see Table 3) were taken for NP-AA-M/H (medium and high DSs) and NP-AA-HH was synthesized separately (see 4.2.6.1)

For preparation of nanoparticles the solid samples were dissolved in a mixture of acetone/water and centrifuged (5000 rpm, 20 min) to remove undissolved solids first.

For all 10 NP-samples a mixture of acetone/DI water, 3:1, v/v was used for dissolving except the hexanoic lignin ester which needed to be treated with pure acetone due to high non polarity. The obtained solutions were transferred into a dropping funnel and added to DI water (DI water/NP solution, 2:1, v/v) dropwise at a defined rotational speed of 250 rpm. Afterwards acetone was removed under reduced pressure at 60 °C. Just the blank sample (NP-native) couldn't be handled because of uncontrollable retardation whilst evaporation and thus was placed in the fume hood for acetone evaporation overnight. A solid content of 0.4 wt% was determined for the native nanoparticle dispersion. In order to work with a constant amount of solid nanoparticles in further analysis, all other nanoparticle dispersions were adjusted to a solid content of 0.4 wt% as well. Therefore, a defined amount of sample (2-4 g) was transferred into an aluminum weighting cup and dried for 3 h at 105 °C until no solvent residue was left. Subsequent weighting at temperature constant conditions leads to a certain amount of sample in a defined amount of suspension. This procedure was replicated twice. The weight percentages were calculated and varying

volumes of DI water were added to the stock solutions achieving a solid content of 0.4 wt% for all nanoparticles.

4.3   Methods: characterization and analysis

4.3.1   Nuclear magnetic resonance spectroscopy (NMR)

^{1}H-NMR experiments were performed on a Bruker Avance II 400 MHz instrument with DMSO-d_6 as solvent. ^{31}P-NMR experiments were carried out on the same instrument, but the frequency was adjusted to 162 MHz. Dissolution of the samples was done by using a mixture of CDCl$_3$/pyridine-d5 followed by derivatization with 2-chloro-4,4,5,5-tetramethyl-1,3-2-dioxaphospholane (TMPD). The parameters were set to: 0.6 s acquisition time, 15 s relaxation delay and 256 scan rate. All data were processed and analyzed with TopSpin 4.1.3 software.

4.3.2   Particle diameter and zeta (ζ) potential analysis (Zetasizer)

Particle diameters (wavelength for DLS = 633 nm) and ζ potential of all nanoparticles were analyzed with Zetasizer Nano ZSP system (Malvern) and DTS0012 (size), DTS1070 (ζ potential) cuvettes respectively. The refractive Index (RI) was set to 1.347 and the samples were measured at 25 °C in a concentration of 0.04 wt% using 100 mM NaCl solution.

4.3.3   Atomic force microscopy (AFM)

Atomic force microscopy (AFM) measurements were performed with Dimension Icon Atomic Force Microscope (Nanoscope V controller, Bruker, USA). The mode was set to ScanAsyst imaging using ScanAsyst-Air tips with a normal tip radius of 2 nm (Bruker). Topographical scans from 2 x 2 μm^2 to 500 x 500 nm^2 with varying pixels of 256 x 256 or 512 x 512 were conducted with a scan rate between 0.1-0.65 Hz. Measurements were carried out on many different locations on the surfaces of the samples which were prepared on either SiO$_2$ wafers or micro slides and investigated in air using trapping mode. Images were processed and manipulated with Gwyddion software.

4.3.4   Fourier transformed infrared spectroscopy (FTIR)

For attenuated total reflection (ATR) FTIR spectroscopy equipped with a ZnSe ATR crystal and LiTaO$_3$ detector a PerkinElmer (PerkinElmer Inc., MA, USA) Frontier IR single-range spectrometer was used. All measurements of solid samples were recorded with 4 scans per minute in the range between 4000 cm^{-1} and 650 cm^{-1} and a resolution of 4 cm^{-1}. Baseline correction to a coarseness of 40% and normalization to 1 at a wavenumber of 1600 cm^{-1} was adjusted using SpectraGryph 1.2 software.

4.3.5 Ultraviolet – visible spectroscopy (UV-VIS)

UV-VIS experiments were done on a Perkin Elmer Lambda 35 instrument in a scan range of 200-800 nm. Scan speed was adjusted to 480 nm min^{-1}, data interval to 1 nm and slit width to 1 nm. A concentration of 0.0025 g L^{-1} in 100 mM NaCl was adjusted for all samples. The spectra were processed via SpectraGryph 1.2 software.

4.3.6 Contact angle (θ) measurement

Contact angle (θ) measurements were carried out on a Drop Shape Analyzer DSA30 (KRÜSS Optronic, Germany) and a syringe with a steel needle (0.51 mm diameter). 3 measurements for each sample were performed on a volume of 5 µL at 20 °C. Dosing speed was adjusted to 3 µL/s and each measurement was recorded at 1 frame per second for 20 s each. Samples (0.04 wt%) were prepared on micro slides by drying 1.3 µL overnight respectively and all data were processed with KRÜSS ADVANCE 1.5.1.0 software using Young Laplace as fitting method.

4.3.7 Pendant Drop measurement

Pendant Drop measurements were carried out on the same instrument as 4.3.6 Contact angle (θ) measurement (Drop Shape Analyzer DSA30, KRÜSS Optronic, Germany) and a syringe with a steel needle (1.83 mm diameter). 3 measurements for each sample were performed on a volume of 13-14 µL depending on the stability of the droplet. Dosing speed was adjusted to 2 µL/s and each measurement was recorded at 0.034 frames per second for 1200 s at 20 °C. All data were processed with KRÜSS ADVANCE 1.5.1.0 software.

4.3.8 Preparation of films and Microscopy

For microscopy analysis an Olympus digital microscope DSX 1000 (Shinjuku, Tokyo, Japan) was used. The zoom was applied to 3 times and 20 times respectively. Samples were prepared by dropping 1 ml 0.4 wt% NP dispersions on micro cover glasses (prewashed with DI water and acetone), followed by subsequent drying in the fume hood overnight.

5 Conclusion and outlook

The solid-solid, solvent free acetylation method with *N*-acetylimidazole and Indulin carried out in a ball mill could be implemented successfully. A straightforward and simple evaluation method based on ^{1}H NMR analysis was developed in order to determine the DS. The resulting DS for 26 runs with varying parameters showed adequate conversions (highest DS 57.33%) considering the accessibility to the aliphatic and aromatic hydroxyl groups of lignin in a heterogeneous reaction. The moisture content of lignin was adjusted intentionally, which implicates that the syntheses were performed forgo preheating. Besides moisture content, reaction time and amount of acetylation agent (*N*-acetylimidazole) were set as varying parameters for optimization in a DoE. Highest addition of *N*-acetylimidazole and a moisture content of 17.25% were determined as optimal conditions, whereas reaction time showed no significant influence on the DS.

The ball mill method was transferred to the solvent free *in situ* method, which is designed to synthesize *N*-acetylimidazole with AA and Im *in situ* followed by its subsequent interaction with lignin. The highest DS of 80.12% was achieved due to a better accessibility of hydroxyl groups in a liquid AA media. Best conditions for the amounts of reactants revealed the highest amount of AA with adapted optimized condition of the ball mill method. Variations in Im amount did not have a large influence on the DS.

Further extension of *in situ* method was done by implementing IBA and HA. Based on the optimized conditions, lignin esters with calculated DS (medium and high) were obtained successfully.

For very high DS it has to be reverted to (Thielemans and Wool, 2004). In total, three different lignin esters with medium, high and very high DS respectively were prepared and used for nanoparticle precipitation.

The LNP particle size analysis, performed by accessing ζ Potential and via UV-VIS measurements showed similar results compared to the unmodified sample.

Spherical morphology and smaller sizes than NP-native was determined for all NP esters. The sizes for modified LNP esters ascended corresponding to the dimensions of the respective ester groups.

Rough surfaces with cracks, elongated partly rising areas and a square microstructure with mostly centered nanoparticles developed through film preparation for optical analysis. These micro slides were also used for contact angle (θ)

measurements at which NP-HA-HH present most intense hydrophobic properties but all samples showed a slight increase of θ compared to NP-native. Therefore, a core-shell structure with mostly hydrophilic functional groups on the surface and hydrophobic groups centered in the core, resulting from the NP preparation process, was assumed. Surface analysis via pendant drop strengthened the presumption, because all LNP esters showed lower surface tension than water though higher (or similar) surface tension than NP-native.

The prepared NPs demonstrate properties favorable for using them as reinforced phase in hydrophobic matrices of plastic or hybrid nanocapsules in phase change materials. For this purpose fatty acids (more hydrophobic esters) or longer non polar esters as used might be necessary in order to enhance hydrophobicity.

The applied method for esterification with different anhydride could also be improved with the object of replacing this toxic chemical ideally for a non-toxic chemical comparable impact.

Specifically for this thesis, analysis for thermal properties such as DSC would have given interesting information on the stability and glass transition. Lacking of highly defined AFM pictures with lower concentration made size and morphology determination challenging which could also be improved using different settings or instruments such as transmission electron microscopy (TEM).

Nevertheless, the used concepts and methods offered easy and environmentally friendly routes for acetylation and esterification of lignin. Even hampering water for most acetylation processes was integrated into a reaction scheme successfully and therefore preventing energy intensive pre-drying. The exploitation of lignin with solvent free syntheses and good scale-up possibilities are feasible with moderate effort and high outcome.

6 Literature

Abushammala, H., Hettegger, H., Bacher, M., Korntner, P., Potthast, A., Rosenau, T., Laborie, M.-P., 2017. On the mechanism of the unwanted acetylation of polysaccharides by 1,3-dialkylimidazolium acetate ionic liquids: part 2—the impact of lignin on the kinetics of cellulose acetylation. Cellulose 24, 2767–2774. https://doi.org/10.1007/s10570-017-1322-x

Achyuthan, K.E., Achyuthan, A.M., Adams, P.D., Dirk, S.M., Harper, J.C., Simmons, B.A., Singh, A.K., 2010. Supramolecular Self-Assembled Chaos: Polyphenolic Lignin's Barrier to Cost-Effective Lignocellulosic Biofuels. Molecules 15, 8641–8688. https://doi.org/10.3390/molecules15118641

Ahvazi, B., Cloutier, É., Wojciechowicz, O., Ngo, T.-D., 2016. Lignin Profiling: A Guide for Selecting Appropriate Lignins as Precursors in Biomaterials Development. ACS Sustainable Chem. Eng. 4, 5090–5105. https://doi.org/10.1021/acssuschemeng.6b00873

An, L., Si, C., Wang, G., Choi, C.S., Yu, Y.H., Bae, J.H., Lee, S.M., Kim, Y.S., 2019. Efficient and green approach for the esterification of lignin with oleic acid using surfactant-combined microreactors in water. BioRes 15, 89–104. https://doi.org/10.15376/biores.15.1.89-104

Antonino, L.D., Gouveia, J.R., de Sousa Júnior, R.R., Garcia, G.E.S., Gobbo, L.C., Tavares, L.B., dos Santos, D.J., 2021. Reactivity of Aliphatic and Phenolic Hydroxyl Groups in Kraft Lignin towards 4,4′ MDI. Molecules 26, 2131. https://doi.org/10.3390/molecules26082131

Anwar, Z., Gulfraz, M., Irshad, M., 2014. Agro-industrial lignocellulosic biomass a key to unlock the future bio-energy: A brief review. Journal of Radiation Research and Applied Sciences 7, 163–173. https://doi.org/10.1016/j.jrras.2014.02.003

Argyropoulos, D., 1994. Quantitative Phosphorus-31 NMR Analysis of Lignins, a New Tool for the Lignin Chemist. J. of Wood Chem. & Tech. 14, 45–63. https://doi.org/10.1080/02773819408003085

Azimvand, J., Didehban, K., Mirshokraie, S., 2018. Safranin-O removal from aqueous solutions using lignin nanoparticle-g-polyacrylic acid adsorbent: Synthesis, properties, and application. Adsorption Science & Technology 36, 1422–1440. https://doi.org/10.1177/0263617418777836

Balakshin, M.Yu., Capanema, E.A., 2015. Comprehensive structural analysis of biorefinery lignins with a quantitative ^{13}C NMR approach. RSC Adv. 5, 87187–87199. https://doi.org/10.1039/C5RA16649G

Beaumont, M., Jusner, P., Gierlinger, N., King, A.W.T., Potthast, A., Rojas, O.J., Rosenau, T., 2021. Unique reactivity of nanoporous cellulosic materials mediated by surface-confined water. Nat Commun 12, 2513. https://doi.org/10.1038/s41467-021-22682-3

Beaumont, M., Winklehner, S., Veigel, S., Mundigler, N., Gindl-Altmutter, W., Potthast, A., Rosenau, T., 2020. Wet esterification of never-dried cellulose: a simple process to surface-acetylated cellulose nanofibers. Green Chem. 22, 5605–5609. https://doi.org/10.1039/D0GC02116D

Behin, J., Sadeghi, N., 2016. Utilization of waste lignin to prepare controlled-slow release urea. Int J Recycl Org Waste Agricult 5, 289–299. https://doi.org/10.1007/s40093-016-0139-1

Behling, R., Valange, S., Chatel, G., 2016. Heterogeneous catalytic oxidation for lignin valorization into valuable chemicals: what results? What limitations? What trends? Green Chem. 18, 1839–1854. https://doi.org/10.1039/C5GC03061G

Bertella, S., Luterbacher, J.S., 2020. Lignin Functionalization for the Production of Novel Materials. Trends in Chemistry 2, 440–453. https://doi.org/10.1016/j.trechm.2020.03.001

Betts, W.B., Dart, R.K., Ball, A.S., Pedlar, S.L., 1991. Biosynthesis and Structure of Lignocellulose, in: Betts, W.B. (Ed.), Biodegradation, Springer Series in Applied Biology. Springer London, London, pp. 139–155. https://doi.org/10.1007/978-1-4471-3470-1_7

Boerjan, W., Ralph, J., Baucher, M., 2003. Lignin Biosynthesis. Annu. Rev. Plant Biol. 54, 519–546. https://doi.org/10.1146/annurev.arplant.54.031902.134938

Carvajal, J.C., Gómez, Á., Cardona, C.A., 2016. Comparison of lignin extraction processes: Economic and environmental assessment. Bioresource Technology 214, 468–476. https://doi.org/10.1016/j.biortech.2016.04.103

Cong, H., Cao, W., 2004. Thin Film Interference of Colloidal Thin Films. Langmuir 20, 8049–8053. https://doi.org/10.1021/la049118+

Crestini, C., Lange, H., Sette, M., Argyropoulos, D.S., 2017. On the structure of softwood kraft lignin. Green Chem. 19, 4104–4121. https://doi.org/10.1039/C7GC01812F

Dai, L., Liu, R., Hu, L.-Q., Zou, Z.-F., Si, C.-L., 2017. Lignin Nanoparticle as a Novel Green Carrier for the Efficient Delivery of Resveratrol. ACS Sustainable Chem. Eng. 5, 8241–8249. https://doi.org/10.1021/acssuschemeng.7b01903

Dapsens, P.Y., Mondelli, C., Pérez-Ramírez, J., 2012. Biobased Chemicals from Conception toward Industrial Reality: Lessons Learned and To Be Learned. ACS Catal. 2, 1487–1499. https://doi.org/10.1021/cs300124m

Deng, Y., Feng, X., Zhou, M., Qian, Y., Yu, H., Qiu, X., 2011. Investigation of Aggregation and Assembly of Alkali Lignin Using Iodine as a Probe. Biomacromolecules 12, 1116–1125. https://doi.org/10.1021/bm101449b

Dessbesell, L., Paleologou, M., Leitch, M., Pulkki, R., Xu, C. (Charles), 2020. Global lignin supply overview and kraft lignin potential as an alternative for petroleum-based polymers. Renewable and Sustainable Energy Reviews 123, 109768. https://doi.org/10.1016/j.rser.2020.109768

Dittenber, D.B., GangaRao, H.V.S., 2012. Critical review of recent publications on use of natural composites in infrastructure. Composites Part A: Applied Science and Manufacturing 43, 1419–1429. https://doi.org/10.1016/j.compositesa.2011.11.019

Doherty, W.O.S., Mousavioun, P., Fellows, C.M., 2011. Value-adding to cellulosic ethanol: Lignin polymers. Industrial Crops and Products 33, 259–276. https://doi.org/10.1016/j.indcrop.2010.10.022

Farooq, M., Zou, T., Riviere, G., Sipponen, M.H., Österberg, M., 2019. Strong, Ductile, and Waterproof Cellulose Nanofibril Composite Films with Colloidal Lignin Particles. Biomacromolecules 20, 693–704. https://doi.org/10.1021/acs.biomac.8b01364

Figueiredo, P., Lintinen, K., Hirvonen, J.T., Kostiainen, M.A., Santos, H.A., 2018. Properties and chemical modifications of lignin: Towards lignin-based nanomaterials for biomedical applications. Progress in Materials Science 93, 233–269. https://doi.org/10.1016/j.pmatsci.2017.12.001

Fox, S.C., McDonald, A.G., 2010. CHEMICAL AND THERMAL CHARACTERIZATION OF THREE INDUSTRIAL LIGNINS AND THEIR CORRESPONDING LIGNIN ESTERS 20.

Gao, W., Fatehi, P., 2019. Lignin for polymer and nanoparticle production: Current status and challenges. Can. J. Chem. Eng. 97, 2827–2842. https://doi.org/10.1002/cjce.23620

Gilca, I.A., Popa, V.I., Crestini, C., 2015. Obtaining lignin nanoparticles by sonication. Ultrasonics Sonochemistry 23, 369–375. https://doi.org/10.1016/j.ultsonch.2014.08.021

Glasser, W.G., Jain, R.K., 1993. Lignin Derivatives. I. Alkanoates. hfsg 47, 225–233. https://doi.org/10.1515/hfsg.1993.47.3.225

Gosselink, R.J.A., 2011. Lignin as a renewable aromatic resource for the chemical industry.

Guerra, A., Filpponen, I., Lucia, L.A., Argyropoulos, D.S., 2006. Comparative Evaluation of Three Lignin Isolation Protocols for Various Wood Species. J. Agric. Food Chem. 54, 9696–9705. https://doi.org/10.1021/jf062433c

H. Clark, J., E. I. Deswarte, F., J. Farmer, T., 2009. The integration of green chemistry into future biorefineries. Biofuels, Bioprod. Bioref. 3, 72–90. https://doi.org/10.1002/bbb.119

Haq, I., Mazumder, P., Kalamdhad, A.S., 2020. Recent advances in removal of lignin from paper industry wastewater and its industrial applications – A review. Bioresource Technology 312, 123636. https://doi.org/10.1016/j.biortech.2020.123636

Hassan, S.S., Williams, G.A., Jaiswal, A.K., 2018. Emerging technologies for the pretreatment of lignocellulosic biomass. Bioresource Technology 262, 310–318. https://doi.org/10.1016/j.biortech.2018.04.099

Hatfield, R., Vermerris, W., 2001. Lignin Formation in Plants. The Dilemma of Linkage Specificity. Plant Physiology 126, 1351–1357. https://doi.org/10.1104/pp.126.4.1351

He, X., Luzi, F., Yang, W., Xiao, Z., Torre, L., Xie, Y., Puglia, D., 2018. Citric Acid as Green Modifier for Tuned Hydrophilicity of Surface Modified Cellulose and Lignin Nanoparticles. ACS Sustainable Chem. Eng. 6, 9966–9978. https://doi.org/10.1021/acssuschemeng.8b01202

Hu, Z., Yeh, T.-F., Chang, H., Matsumoto, Y., Kadla, J.F., 2006. Elucidation of the structure of cellulolytic enzyme lignin. Holzforschung 60, 389–397. https://doi.org/10.1515/HF.2006.061

Huang, J., Fu, S., Gan, L., 2019. Lignin Chemistry and Applications. Elsevier.

Huber, G.W., Corma, A., 2007. Synergies between Bio- and Oil Refineries for the Production of Fuels from Biomass. Angew. Chem. Int. Ed. 46, 7184–7201. https://doi.org/10.1002/anie.200604504

Iwata, T., 2015. Biodegradable and Bio-Based Polymers: Future Prospects of Eco-Friendly Plastics. Angew. Chem. Int. Ed. 54, 3210–3215. https://doi.org/10.1002/anie.201410770

Kai, D., Ren, W., Tian, L., Chee, P.L., Liu, Y., Ramakrishna, S., Loh, X.J., 2016. Engineering Poly(lactide)–Lignin Nanofibers with Antioxidant Activity for Biomedical Application. ACS Sustainable Chem. Eng. 4, 5268–5276. https://doi.org/10.1021/acssuschemeng.6b00478

Kai, X., Can, J., GuiFeng, L., GuoMing, W., Jian, C., ZhenWu, K., 2015. Preparation and characterization of lignin nanoparticles with controllable size by nanoprecipitation method. Chemistry and Industry of Forest Products 35, 85–92.

Khan, A.A., de Jong, W., Jansens, P.J., Spliethoff, H., 2009. Biomass combustion in fluidized bed boilers: Potential problems and remedies. Fuel Processing Technology 90, 21–50. https://doi.org/10.1016/j.fuproc.2008.07.012

Kumar, N., Sharma, A., 2021. Nano-Forensics: The New Perspective in Precision Forensic Science, in: Saglam, N., Korkusuz, F., Prasad, R. (Eds.), Nanotechnology Applications in Health and Environmental Sciences. Springer

International Publishing, Cham, pp. 111–134. https://doi.org/10.1007/978-3-030-64410-9_6

Lee, R.A., Bédard, C., Berberi, V., Beauchet, R., Lavoie, J.-M., 2013. UV–Vis as quantification tool for solubilized lignin following a single-shot steam process. Bioresource Technology 144, 658–663. https://doi.org/10.1016/j.biortech.2013.06.045

Lewis, H.F., Brauns, F.E., Buchanan, M.A., Brookbank, E.B., 1943. Lignin Esters of Mono- and Dibasic Aliphatic Acids. Ind. Eng. Chem. 35, 1113–1117. https://doi.org/10.1021/ie50406a020

Li, C., Zhao, X., Wang, A., Huber, G.W., Zhang, T., 2015. Catalytic Transformation of Lignin for the Production of Chemicals and Fuels. Chem. Rev. 115, 11559–11624. https://doi.org/10.1021/acs.chemrev.5b00155

Li, T., Yin, Y., Wu, S., Ma, H., Zhang, F., 2020. Effect of pre-acetylation of hydroxyl functional groups by choline chloride/acetic anhydride on subsequent lignin pyrolysis. Bioresource Technology 317, 124034. https://doi.org/10.1016/j.biortech.2020.124034

Liao, J.J., Latif, N.H.A., Trache, D., Brosse, N., Hussin, M.H., 2020. Current advancement on the isolation, characterization and application of lignin. International Journal of Biological Macromolecules 162, 985–1024. https://doi.org/10.1016/j.ijbiomac.2020.06.168

Lievonen, M., Valle-Delgado, J.J., Mattinen, M.-L., Hult, E.-L., Lintinen, K., Kostiainen, M.A., Paananen, A., Szilvay, G.R., Setälä, H., Österberg, M., 2016. A simple process for lignin nanoparticle preparation. Green Chem. 18, 1416–1422. https://doi.org/10.1039/C5GC01436K

Lin, C.S.K., Pfaltzgraff, L.A., Herrero-Davila, L., Mubofu, E.B., Abderrahim, S., Clark, J.H., Koutinas, A.A., Kopsahelis, N., Stamelatou, K., Dickson, F., Thankappan, S., Mohamed, Z., Brocklesby, R., Luque, R., 2013. Food waste as a valuable resource for the production of chemicals, materials and fuels. Current situation and global perspective. Energy Environ. Sci. 6, 426. https://doi.org/10.1039/c2ee23440h

Liu, Z.-H., Hao, N., Shinde, S., Olson, M.L., Bhagia, S., Dunlap, J.R., Kao, K.C., Kang, X., Ragauskas, A.J., Yuan, J.S., 2019a. Codesign of Combinatorial Organosolv Pretreatment (COP) and Lignin Nanoparticles (LNPs) in Biorefineries. ACS Sustainable Chem. Eng. 7, 2634–2647. https://doi.org/10.1021/acssuschemeng.8b05715

Liu, Z.-H., Hao, N., Shinde, S., Pu, Y., Kang, X., Ragauskas, A.J., Yuan, J.S., 2019b. Defining lignin nanoparticle properties through tailored lignin reactivity by sequential organosolv fragmentation approach (SOFA). Green Chem. 21, 245–260. https://doi.org/10.1039/C8GC03290D

Margarida Martins, M., Carvalheiro, F., Gírio, F., 2022. An overview of lignin pathways of valorization: from isolation to refining and conversion into value-added products. Biomass Conv. Bioref. https://doi.org/10.1007/s13399-022-02701-z

Monteil-Rivera, F., Paquet, L., 2015. Solvent-free catalyst-free microwave-assisted acylation of lignin. Industrial Crops and Products 65, 446–453. https://doi.org/10.1016/j.indcrop.2014.10.060

Nothling, M.D., Ganesan, A., Condic-Jurkic, K., Pressly, E., Davalos, A., Gotrik, M.R., Xiao, Z., Khoshdel, E., Hawker, C.J., O'Mara, M.L., Coote, M.L., Connal, L.A., 2017. Simple Design of an Enzyme-Inspired Supported Catalyst Based on a Catalytic Triad. Chem 2, 732–745. https://doi.org/10.1016/j.chempr.2017.04.004

Österberg, M., Sipponen, M.H., Mattos, B.D., Rojas, O.J., 2020. Spherical lignin particles: a review on their sustainability and applications. Green Chem. 22, 2712–2733. https://doi.org/10.1039/D0GC00096E

Qian, Y., Deng, Y., Qiu, X., Li, H., Yang, D., 2014. Formation of uniform colloidal spheres from lignin, a renewable resource recovered from pulping spent liquor. Green Chem. 16, 2156. https://doi.org/10.1039/c3gc42131g

Ragauskas, A.J., Beckham, G.T., Biddy, M.J., Chandra, R., Chen, F., Davis, M.F., Davison, B.H., Dixon, R.A., Gilna, P., Keller, M., Langan, P., Naskar, A.K., Saddler, J.N., Tschaplinski, T.J., Tuskan, G.A., Wyman, C.E., 2014. Lignin Valorization: Improving Lignin Processing in the Biorefinery. Science 344, 1246843. https://doi.org/10.1126/science.1246843

Ralph, J., Lapierre, C., Boerjan, W., 2019. Lignin structure and its engineering. Current Opinion in Biotechnology 56, 240–249. https://doi.org/10.1016/j.copbio.2019.02.019

Ralph, J., Lundquist, K., Brunow, G., Lu, F., Kim, H., Schatz, P.F., Marita, J.M., Hatfield, R.D., Ralph, S.A., Christensen, J.H., Boerjan, W., 2004. Lignins: Natural polymers from oxidative coupling of 4-hydroxyphenyl- propanoids. Phytochemistry Reviews 3, 29–60. https://doi.org/10.1023/B:PHYT.0000047809.65444.a4

Reesi, F., Minaiyan, M., Taheri, A., 2018. A novel lignin-based nanofibrous dressing containing arginine for wound-healing applications. Drug Deliv. and Transl. Res. 8, 111–122. https://doi.org/10.1007/s13346-017-0441-0

Richter, A.P., Bharti, B., Armstrong, H.B., Brown, J.S., Plemmons, D., Paunov, V.N., Stoyanov, S.D., Velev, O.D., 2016. Synthesis and Characterization of Biodegradable Lignin Nanoparticles with Tunable Surface Properties. Langmuir 32, 6468–6477. https://doi.org/10.1021/acs.langmuir.6b01088

Rodrigues Mota, T., Matias de Oliveira, D., Marchiosi, R., Ferrarese-Filho, O., Dantas dos Santos, W., Laboratory of Plant Biochemistry, Department of Biochemistry, State University of Maringá, PR, Brazil, † These authors contributed equally to this work., 2018. Plant cell wall composition and enzymatic deconstruction. AIMS Bioengineering 5, 63–77. https://doi.org/10.3934/bioeng.2018.1.63

Sabine, C.L., Feely, R.A., Gruber, N., Key, R.M., Lee, K., Bullister, J.L., Wanninkhof, R., Wong, C.S., Wallace, D.W.R., Tilbrook, B., Millero, F.J., Peng, T.-H., Kozyr, A., Ono, T., Rios, A.F., 2004. The Oceanic Sink for Anthropogenic CO_2. Science 305, 367–371. https://doi.org/10.1126/science.1097403

Saratale, R.G., Saratale, G.D., Ghodake, G., Cho, S.-K., Kadam, A., Kumar, G., Jeon, B.-H., Pant, D., Bhatnagar, A., Shin, H.S., 2019. Wheat straw extracted lignin in silver nanoparticles synthesis: Expanding its prophecy towards antineoplastic potency and hydrogen peroxide sensing ability. International Journal of Biological Macromolecules 128, 391–400. https://doi.org/10.1016/j.ijbiomac.2019.01.120

Sarkanen, S., Teller, D.C., Abramowski, E., McCarthy, J.L., 1982. Lignin. 19. Kraft lignin component conformation and associated complex configuration in aqueous alkaline solution. Macromolecules 15, 1098–1104. https://doi.org/10.1021/ma00232a027

Schneider, W.D.H., Bolaño Losada, C., Moldes, D., Fontana, R.C., de Siqueira, F.G., Prieto, A., Martínez, M.J., Martínez, Á.T., Dillon, A.J.P., Camassola, M., 2019. A Sustainable Approach of Enzymatic Grafting on *Eucalyptus globulus* Wood by Laccase from the Newly Isolated White-Rot Basidiomycete *Marasmiellus*

palmivorus VE111. ACS Sustainable Chem. Eng. 7, 13418–13424. https://doi.org/10.1021/acssuschemeng.9b02770

Schneider, W.D.H., Dillon, A.J.P., Camassola, M., 2021. Lignin nanoparticles enter the scene: A promising versatile green tool for multiple applications. Biotechnology Advances 47, 107685. https://doi.org/10.1016/j.biotechadv.2020.107685

Setälä, H., Alakomi, H.-L., Paananen, A., Szilvay, G.R., Kellock, M., Lievonen, M., Liljeström, V., Hult, E.-L., Lintinen, K., Österberg, M., Kostiainen, M., 2020. Lignin nanoparticles modified with tall oil fatty acid for cellulose functionalization. Cellulose 27, 273–284. https://doi.org/10.1007/s10570-019-02771-9

Sipponen, M.H., Henn, A., Penttilä, P., Österberg, M., 2020. Lignin-fatty acid hybrid nanocapsules for scalable thermal energy storage in phase-change materials. Chemical Engineering Journal 393, 124711. https://doi.org/10.1016/j.cej.2020.124711

Sipponen, M.H., Lange, H., Ago, M., Crestini, C., 2018. Understanding Lignin Aggregation Processes. A Case Study: Budesonide Entrapment and Stimuli Controlled Release from Lignin Nanoparticles. ACS Sustainable Chem. Eng. 6, 9342–9351. https://doi.org/10.1021/acssuschemeng.8b01652

Tang, Q., Qian, Y., Yang, D., Qiu, X., Qin, Y., Zhou, M., 2020. Lignin-Based Nanoparticles: A Review on Their Preparations and Applications. Polymers 12, 2471. https://doi.org/10.3390/polym12112471

Thielemans, W., Wool, R.P., 2005. Lignin Esters for Use in Unsaturated Thermosets: Lignin Modification and Solubility Modeling. Biomacromolecules 6, 1895–1905. https://doi.org/10.1021/bm0500345

Thielemans, W., Wool, R.P., 2004. Butyrated kraft lignin as compatibilizing agent for natural fiber reinforced thermoset composites. Composites Part A: Applied Science and Manufacturing 35, 327–338. https://doi.org/10.1016/j.compositesa.2003.09.011

Tian, D., Hu, J., Chandra, R.P., Saddler, J.N., Lu, C., 2017. Valorizing Recalcitrant Cellulolytic Enzyme Lignin via Lignin Nanoparticles Fabrication in an Integrated Biorefinery. ACS Sustainable Chem. Eng. 5, 2702–2710. https://doi.org/10.1021/acssuschemeng.6b03043

Tinnemans, A.H.A., Greidanus, P.J., 1984. Chemically modified lignin for use in polymer blends. (Comm. Eur. Communities).

Trevisan, H., Rezende, C.A., 2020. Pure, stable and highly antioxidant lignin nanoparticles from elephant grass. Industrial Crops and Products 145, 112105. https://doi.org/10.1016/j.indcrop.2020.112105

Upton, B.M., Kasko, A.M., 2016. Strategies for the Conversion of Lignin to High-Value Polymeric Materials: Review and Perspective. Chem. Rev. 116, 2275–2306. https://doi.org/10.1021/acs.chemrev.5b00345

Vance, C.P., Kirk, T.K., Sherwood, R.T., 1980. Lignification as a Mechanism of Disease Resistance. Annu. Rev. Phytopathol. 18, 259–288. https://doi.org/10.1146/annurev.py.18.090180.001355

Vinardell, M., Mitjans, M., 2017. Lignins and Their Derivatives with Beneficial Effects on Human Health. IJMS 18, 1219. https://doi.org/10.3390/ijms18061219

Wang, B., Sun, D., Wang, H.-M., Yuan, T.-Q., Sun, R.-C., 2019. Green and Facile Preparation of Regular Lignin Nanoparticles with High Yield and Their Natural Broad-Spectrum Sunscreens. ACS Sustainable Chem. Eng. 7, 2658–2666. https://doi.org/10.1021/acssuschemeng.8b05735

Wang, C., Kelley, S.S., Venditti, R.A., 2016. Lignin-Based Thermoplastic Materials. ChemSusChem 9, 770–783. https://doi.org/10.1002/cssc.201501531

Wang, G., Xia, Y., Sui, W., Si, C., 2018. Lignin as a Novel Tyrosinase Inhibitor: Effects of Sources and Isolation Processes. ACS Sustainable Chem. Eng. 6, 9510–9518. https://doi.org/10.1021/acssuschemeng.8b02234

Wang, H., Pu, Y., Ragauskas, A., Yang, B., 2019. From lignin to valuable products–strategies, challenges, and prospects. Bioresource Technology 271, 449–461. https://doi.org/10.1016/j.biortech.2018.09.072

Wang, X., Nakamoto, T., Dulińska-Molak, I., Kawazoe, N., Chen, G., 2016. Regulating the stemness of mesenchymal stem cells by tuning micropattern features. J. Mater. Chem. B 4, 37–45. https://doi.org/10.1039/C5TB02215K

Willner, I., Willner, B., 2010. Biomolecule-Based Nanomaterials and Nanostructures. Nano Lett. 10, 3805–3815. https://doi.org/10.1021/nl102083j

Wong, T.-S., Chen, T.-H., Shen, X., Ho, C.-M., 2011. Nanochromatography Driven by the Coffee Ring Effect. Anal. Chem. 83, 1871–1873. https://doi.org/10.1021/ac102963x

Yang, W., Fortunati, E., Dominici, F., Giovanale, G., Mazzaglia, A., Balestra, G.M., Kenny, J.M., Puglia, D., 2016. Synergic effect of cellulose and lignin nanostructures in PLA based systems for food antibacterial packaging. European Polymer Journal 79, 1–12. https://doi.org/10.1016/j.eurpolymj.2016.04.003

Zhang, Z., Terrasson, V., Guénin, E., 2021. Lignin Nanoparticles and Their Nanocomposites. Nanomaterials 11, 1336. https://doi.org/10.3390/nano11051336

Zhang, Z., Zhang, Y., Lin, Z., Mulyadi, A., Mu, W., Deng, Y., 2017. Butyric anhydride modified lignin and its oil-water interfacial properties. Chemical Engineering Science 165, 55–64. https://doi.org/10.1016/j.ces.2017.02.025

Zhao, W., Simmons, B., Singh, S., Ragauskas, A., Cheng, G., 2016. From lignin association to nano-/micro-particle preparation: extracting higher value of lignin. Green Chem. 18, 5693–5700. https://doi.org/10.1039/C6GC01813K

Zhao, W., Xiao, L.-P., Song, G., Sun, R.-C., He, L., Singh, S., Simmons, B.A., Cheng, G., 2017. From lignin subunits to aggregates: insights into lignin solubilization. Green Chem. 19, 3272–3281. https://doi.org/10.1039/C7GC00944E

Zhao, X., Huang, Z., Zhang, Y., Yang, M., Chen, D., Huang, K., Hu, H., Huang, A., Qin, X., Feng, Z., 2017. Efficient solid-phase synthesis of acetylated lignin and a comparison of the properties of different modified lignins. J. Appl. Polym. Sci. 134. https://doi.org/10.1002/app.44276

Zou, T., Sipponen, M.H., Henn, A., Österberg, M., 2021. Solvent-Resistant Lignin-Epoxy Hybrid Nanoparticles for Covalent Surface Modification and High-Strength Particulate Adhesives. ACS Nano 15, 4811–4823. https://doi.org/10.1021/acsnano.0c09500

Zweckmair, T., Hettegger, H., Abushammala, H., Bacher, M., Potthast, A., Laborie, M.-P., Rosenau, T., 2015. On the mechanism of the unwanted acetylation of polysaccharides by 1,3-dialkylimidazolium acetate ionic liquids: part 1—analysis, acetylating agent, influence of water, and mechanistic considerations. Cellulose 22, 3583–3596. https://doi.org/10.1007/s10570-015-0756-2

Curriculum Vitae

Maximilian Lubitz

Contact: maximilian.lubitz@gmail.com

Personal Information

Date of birth	06 July 1993
Place of birth	Vienna, AT
Nationality	Austria

Work Experience

04/2021 – 10/2021	AUFBAUWERK Bau-, Wohnungs- und Siedlungsgesellschaft m.b.H. Subsidiary of AUFBAU Gemeinnützige Bau-, Wohnungs- und Siedlungsgenossenschaft, office allrounder
08/2015	BIRD-C GmbH – research, laboratory, internship
07/2014	AUFBAU Gemeinnützige Bau-, Wohnungs- und Siedlungs-genossenschaft, Back Office, internship
12/2011 - 08/2012	ÖJAB Hauskrankenpflege Neumargareten, civilian service

Education

2018 - present	Master in Applied Synthetic Chemistry, Vienna University of Technology, 1060 Vienna, AT
2012 – 2018	Bachelor Technical Chemistry, Vienna University of Technology, 1060 Vienna, AT
2003 – 2011	Lise – Meitner Realgymnasium, 1010 Vienna, AT

Focus Vienna University of Technology

Master   Applied Synthetic Chemistry

- Molecular Analysis
- Spectroscopic Methods
- Chemical Analysis of Materials
- Modern 1D and 2D NMR Methods
- Retrosynthesis
- Asymmetric Synthesis
- Industrial Chemistry
- Kinetics and Catalysis
- Food Chemistry and Food Technology
- Ecology and Biochemistry of Plants
- Primary Natural Products from Plants

Master's thesis: "Sustainable Functionalization of Lignin for the Production of Biocolloids"

Bachelor   Technical Chemistry

Bachelor's thesis: "New Chain Transfer Agents for Photopolymerisation"

Focus Lise–Meitner Realgymnasium

- Sciences (Biology, Chemistry, Mathematics, Physics)

Skills and Languages

Languages   German – native proficiency
                           English – good negotiating skills

IT   Microsoft-Office (Excel, Word, Power Point, Outlook)
                           ChemDraw Professional
                           MestReNova
                           Design-Expert

Driving license   B

Activities/Engagement

- Sports activities (tennis, skiing, cycling)
- Traveling (Europe, Australia, America, Southeast Asia)

Maximilian Lubitz